STUDIES ON INNER BREMSSTRAHLUNG OF ^{113}Sn

and

THE RADIOACTIVITY OF NATURAL ROCKS

with

LITHIUM DRIFTED GERMANIUM DETECTORS

A Thesis

Submitted to

the Faculty of Graduate Studies

University of Manitoba

In Partial Fulfillment

of the Requirements for the Degree

MASTER OF SCIENCE

by

Miss NIHAL DAVUDOGLU

September, 1970

Winnipeg, CANADA.

To

Dr. and Mrs. K.I.Roulston

TABLE OF CONTENTS

LIST OF FIGURES

LIST OF TABLES

ACKNOWLEDGEMENTS

The work described in this thesis was carried out at the University of Manitoba, from September, 1968 to September, 1970.

The author is very grateful to late Dr.K.I.Roulston, for so patiently making her interested to the present work. She is particularly grateful to Dr.S.K.Sen, who kindly acted as her supervisor after Dr.K.I.Roulston's untimely death, without whose help and direction this work would have been impossible.

The author wishes to express her sincere thanks to Mr.W.Teoh for his helpful assistance in this work, in particular for his writing the computer programme.

The effort of Dr.A.Chow of Chemistry Department of this University, in purifying the ^{113}Sn source, is greatly appreciated.

A special note of gratitude goes to Dr.R.B.Farguharson for valuable discussion and information as well as the supply of rock samples.

The author also wishes to thank Dr.E.Tomchuk of University of Winnipeg, for kindly letting her use his X-ray spectrometer.

The financial assistance of the National Research Council is gratefully acknowledged.

ABSTRACT

Lithium drifted germanium detectors have extensively been used for spectroscopic studies of ^{113}Sn as well as some rock samples that contain traces of natural radioactive elements Th, U, and K.

The ground state to ground state transition energy of ^{113}In, due to electron capture decay of ^{113}Sn, was determined by measuring the inner bremsstrahlung end-point energy. This was carried out by inner bremsstrahlung X-ray coincidence experiment, using two Ge(Li) detectors. The relative intensity of the 255 keV gamma ray relative to the 393 keV gamma ray, was found to be $(2.9\pm0.3)\times10^{-2}$. The inner bremsstrahlung end-point energy was determined to be 604 keV, giving a ground state to ground state transition energy of 1026 ± 150 keV.

Solid state detectors were used for the first time to investigate the concentration of "trace elements" (Thorium, Uranium, and Potassium) in surface crystalline Canadian rocks. This spectroscopic method provides a non-destructive means of determining the concentrations, and gives much better accuracy than similar work done using NaI crystals. The concentration of the trace elements was inferred by comparision with standard sources prepared in the Earth Science Department of this University, by mixing known amounts of Th, U, and K. The mean concentrations of these trace elements are presented.

CHAPTER I

Ge(Li) DETECTORS

I.1 INTRODUCTION

Spectroscopic investigations of the nucleus began as early as 1911 and up to today the physicists devoted themselves to the laborious task of gathering data, and the field of nuclear spectroscopy grew rapidly. During the "forties" a tremendous effort was put into the development of better instruments and techniques in order that data of higher quality might be obtained.

Lithium drifted germanium gamma-ray detectors were used extensively in the experiments described in this work. When using germanium detectors for gamma-ray spectroscopy, one is concerned primarily with three parameters: energy resolution, time resolution, and counting rate per channel. These are not completely independent parameters, and it is not possible to optimize all three. Generally, the energy resolution is worse with higher counting rates. On the other hand, time resolution is limited by the spread in time required for sufficient charge collection. The total charge released will depend on the total energy expended in ionization. Hence it will depend on both the gamma-ray energy and the mode of

gamma-ray interaction. (See page 8).

The following sections are devoted to a brief discussion of Ge(Li) detectors.

I.2 Ge(Li) SPECTROMETERS

The lithium drift process was first introduced by Pell[1] in order to produce large sensitive volume silicon detectors and was first applied to germanium by Freck and Wakefield[2].

A lithium drifted germanium detector is a solid state ionization device, technically termed a p-i-n structure. (See Fig.I-1). The process consists of evaporating a layer of lithium onto a p-doped germanium crystal and then diffusing it into the crystal to produce an n^+ layer from 100 to 200 μ deep. An electric field is then applied across the p-n junction such that it is reverse biased. The Li^+ ions, which are donors and migrate easily in germanium, are drifted under the influence of this field so that they almost perfectly compensate the acceptors in the p-type material. Thus "intrinsic" layers are produced by compensation and depths of up to 16 mm have been obtained.

At room temperature the leakage current due to thermal agitation of carriers across the band gap (0.67 eV in germanium) prohibits the use of these drifted crystals as spectrometers. Also, at room temperature, the mobility of Li^+ ions is extremely

Figure I-1

Lithium Drifted p-i-n Junction Structure

LITHIUM-DRIFTED p-i-n JUNCTION STRUCTURE

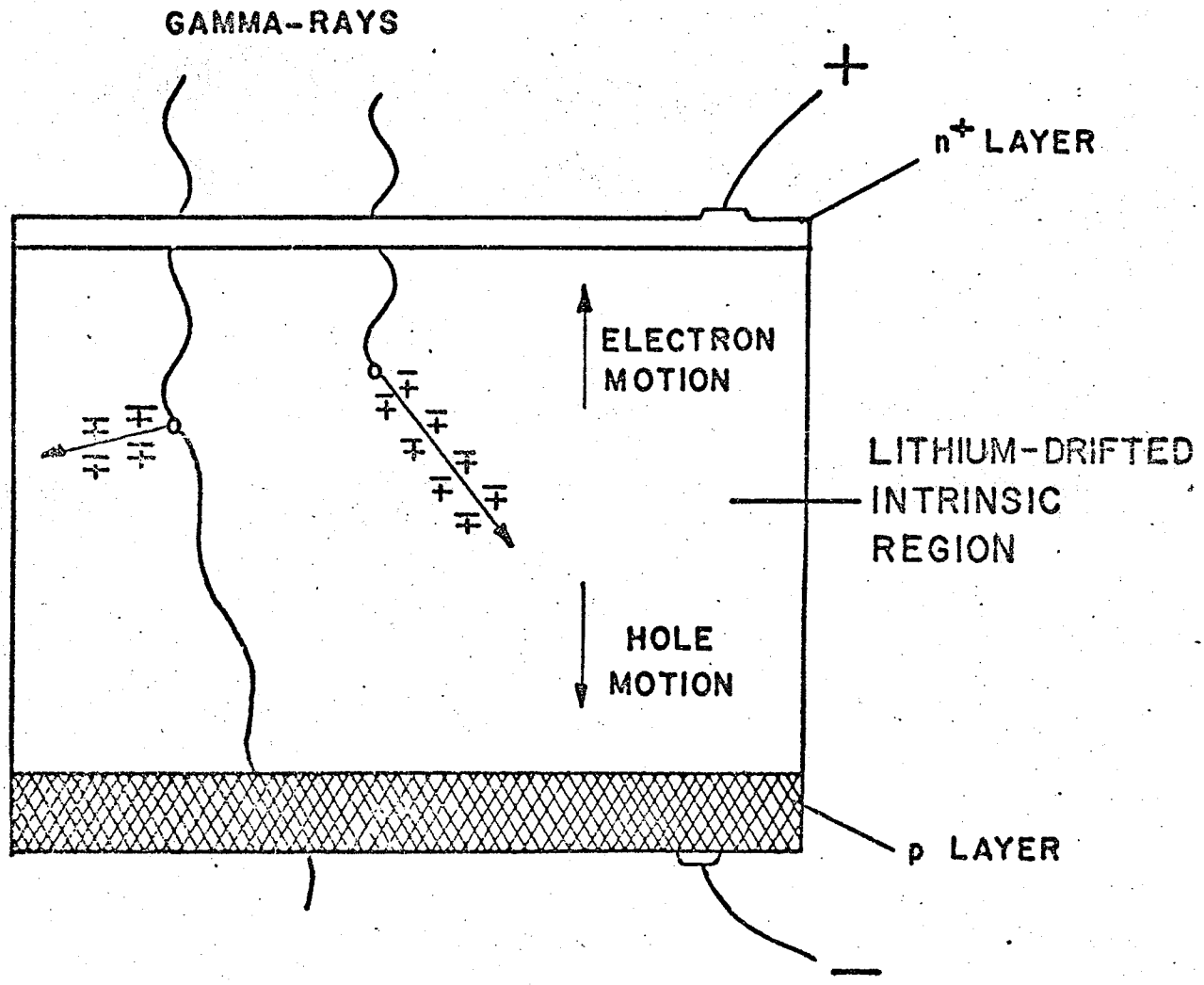

high and unless crystals are cooled, a loss of composition is observed. For these reasons, and the fact that liquid nitrogen is readily obtainable, the detectors are operated at liquid nitrogen temperatures ($77^{\circ}K$) where leakage currents of 10^{-10} and 10^{-11} amperes are not uncommon.

Absorption or scattering of gamma-rays within the intrinsic region produces high speed electrons which lose their energy by creating free charge carriers (electron-hole pairs). These carriers are collected by applying a voltage gradient of the order of 50-100 volt/mm across the intrinsic region and integrating and applying the resultant current. The observed charge spectrum consists of a continuum and one or more narrow peaks from which one can infer the energy spectrum of the incident gamma-ray flux. The area under the peak is a function of the detector size, the shape, and the position of the source with respect to the detector, and the incident photon energy. The mode of the interaction between a gamma ray and the atom within the detector are three:

1) PHOTOELECTRIC INTERACTION: The gamma ray interacts with a K-electron ejecting it from the K shell with energy $E_{\gamma} - E_K$, where E_K is the binding energy of the K-electron. This electron subsequently loses energy by the production of free charge carriers. The X-rays produced by the rearrangement of the orbital electrons filling the K shell vacancy are also absorbed

by the detector, giving a total pulse corresponding to the full energy E_γ. The cross-section for the photoelectric process is proportional to Z^5 and increases rapidly with decreasing photon energy.

2) COMPTON INTERACTION; In this process, the photon is scattered by an electron with a partial energy loss dependent on the angle of scattering. The electron kinetic energy lies between zero and an upper energy limit which depends on the photon energy. The scattering gives rise to a continuous electron-energy distribution between these limits. Cross-section for this process is proportional to the Z of the scattering material.

3) PAIR PRODUCTION: In the vicinity of a nucleus, a gamma-ray energy greater than 1022 keV may produce an electron-positron pair. The electron loses energy by creation of more electron hole pairs. The positron also produces electron hole pairs until it comes to rest, after which it annihilates with another electron producing two 511 keV gamma-rays. If both quanta escape a "double escape" peak is observed with energy $(E_\gamma - 1022)$ keV while if one escapes a "single escape" peak with energy $(E_\gamma - 511)$ keV is observed. Figure I-2 shows the cross-sections of the three processes as a function of energy.

I.3 TYPES OF Ge(Li) DETECTORS

Ge(Li) detectors are of two basic configurations:

Figure I-2

Photoelectric Effect, Compton Scattering

and

Pair Production Cross-Sections in Ge

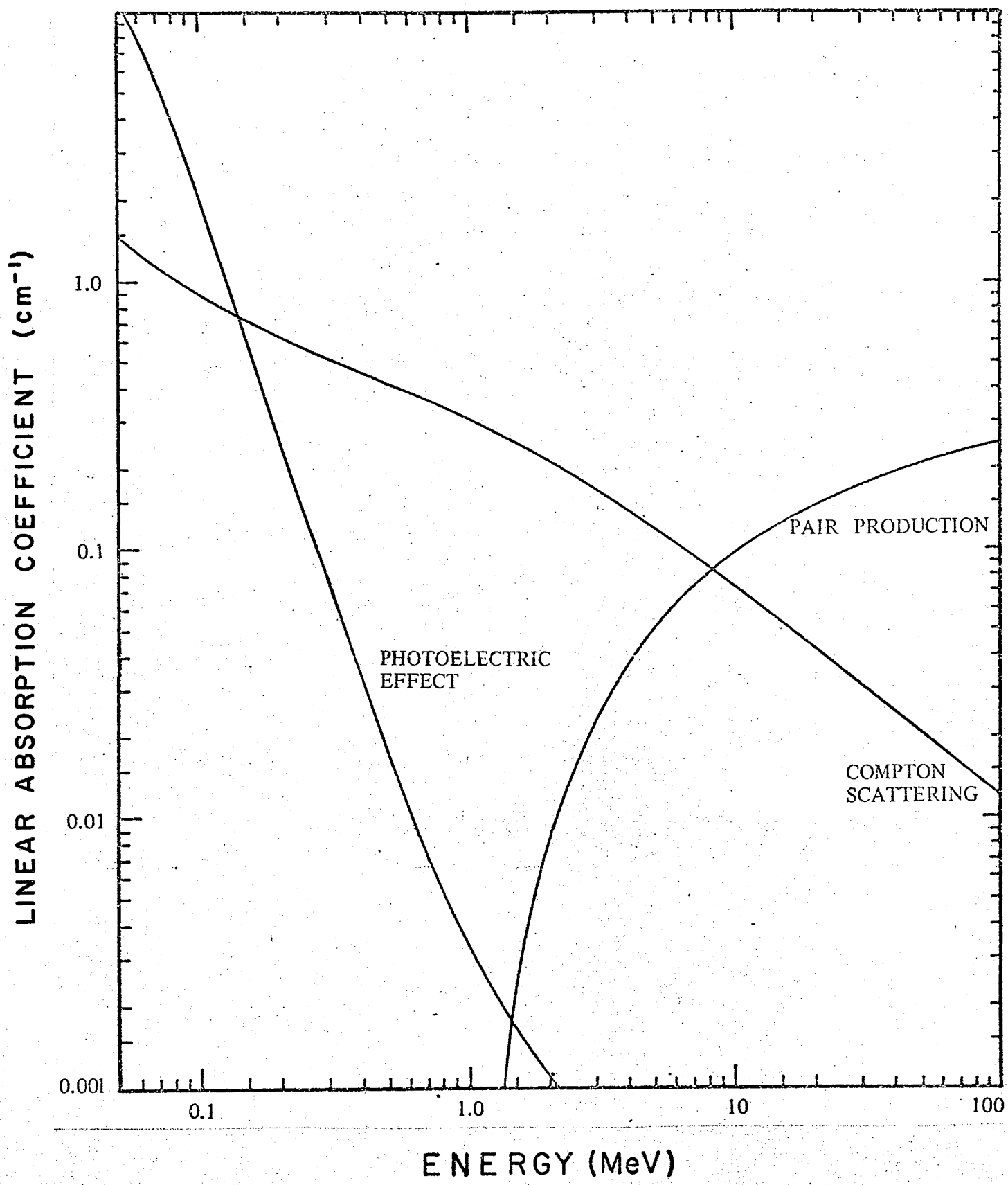
LINEAR ABSORPTION COEFFICIENT (cm⁻¹)
1.0
0.1
0.01
0.001
0.1
1.0
10
100
ENERGY (MeV)
PHOTOELECTRIC EFFECT
PAIR PRODUCTION
COMPTON SCATTERING

PLANAR for finest energy and timing resolution, and true COAXIAL for increased efficiency with excellent timing properties. The detectors are supplied in any of two cryostat configurations: DIP-STICK type and GRAVITY FEED type. (See Fig. I-3). For the dip-stick type cryostat, cooling is achieved by having a cold finger immersed in liquid nitrogen stored in a large-volume dewar. The vacuum chamber surrounding this cold finger is either straight or with a 90^{o} bend. In the chicken-feeder type cryostat, the detector is mounted on the end of a hollow cold finger which is kept filled by gravity with liquid nitrogen from a reservoir above the vacuum chamber.

As a result of the general limitation to the depletion depth, planar detectors are generally available up to a maximum value of about 15 cc. Cylindrical detectors can be made to about 30 cc, and the closed-ended coaxial detectors are available in volumes up to 40 to 50 cc.

The basic limitation of the energy resolution of a Ge(Li) detector is the statistical fluctuation in the number of ion pairs created for a given energy E. This limit involves the Fano factor. Consider a gamma-ray whose energy E is completely absorbed within the intrinsic region of a Ge(Li) detector.

Figure I-3

Detector Cryostat

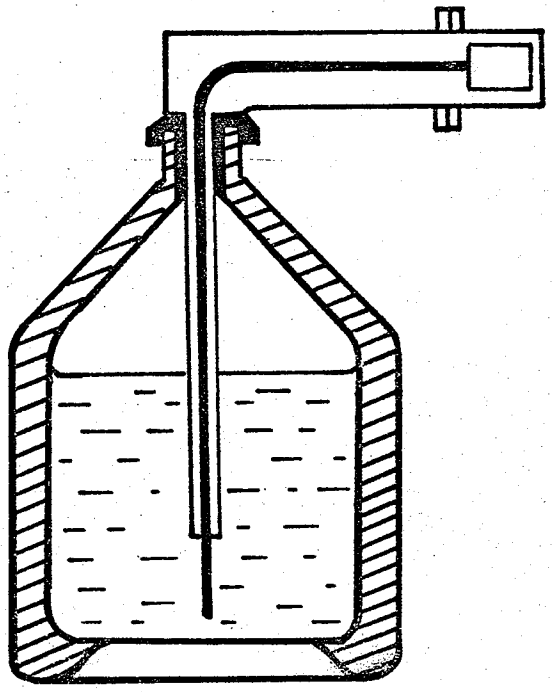

Dipstick cryostat (horizontal)

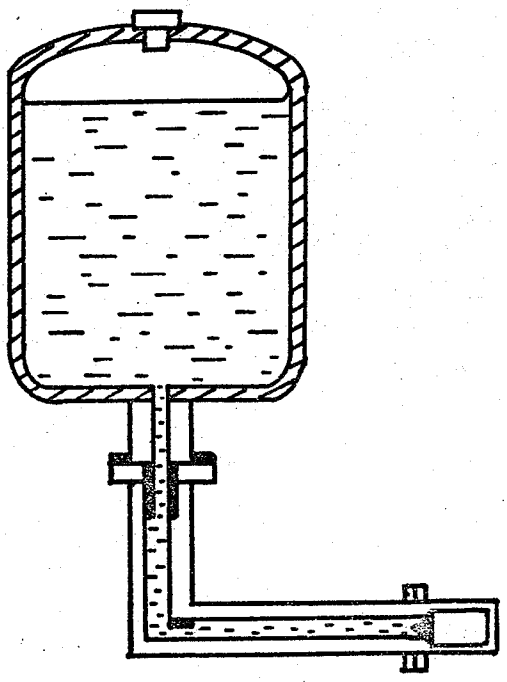

"Chicken-feeder" cryostat (horizontal)

Part of this energy goes into heating the lattice crystal structure. The Fano factor is defined as the ratio of the variance to the yield, as defined below.

The yield is the number of electron-hole pairs produced for a given amount of energy deposition E, while the variance (σ^2) is the mean square variation in the yield. If the average number of electron volts that results in the production of any ion pair in germanium is given by ϵ, then the yield is

$$Y = E/\epsilon$$

and the Fano factor is

$$F = \frac{\sigma^2}{E/\epsilon} \qquad (I,1)$$

To obtain a value for the resolution in keV, (Eq.I.1) is solved for the root mean square variance, σ, and the result converted to electron volts when σ is multiplied by ϵ. This gives

$$\epsilon\sigma = \epsilon\sqrt{\frac{FE}{\epsilon}} = \sqrt{\epsilon EF}$$

The full width at half maximum is obtained by multiplying the result by 2.35, (See Appendix I), hence if ϵ is 2.9×10^{-3} keV/ion pair, then ΔE, the F.W.H.M. expressed in keV for radiation of energy E (keV), becomes

$$\Delta E = 2.35\sqrt{0.0029EF} = 0.1286\sqrt{EF}$$ for germanium at $\sim 77^{\circ}K$.

Table I-1 shows the various energy resolutions of the solid state detectors available in this laboratory.

The following is a very brief review of some of the characteristics of planar and coaxial type Ge(Li) detectors.

PLANAR DETECTORS: Planar detectors are right circular cylinders with the lithium diffused along the long axis in a plane parallel to the circular faces, which serves as the entrance window. The lithium drifted (sensitive) region is adjacent to this face and extends over the full area of the detector. These detectors originally have depletion depths of typically 2 or 3 mm, resulting in low photopeak efficiency and large Compton distribution. Since the Compton distribution serves no useful purpose in gamma-ray spectroscopic measurements, it is desirable to reduce it as much as possible relative to the photopeak height. This can be done by increasing the size of depletion region and hence the active volume.

The planar detectors have an n^+ layer whose thickness can be anything from about 100 μ upwards. This dead layer presents serious attenuation problems when dealing

Table I-1

Ge(Li) Detectors

MANUFACTURER	ACTIVE VOLUME	WINDOW	RESOLUTION (Photon Energy)
PRINCETON γ-TECH.	20 cc.	0·020" Al.	5 keV (1333)
ORTEC	35 cc.	0·5 mm. Al.	2·9 keV (1333)
ORTEC X-ray Spec.	0·25 cc.	0·25 mm. Be.	0·430 keV (14·4)

with low-energy gamma rays. In order to remove this dead layer, the lithium can be drifted right through the p-type material and a surface barrier or diffused p^+ layer can be formed at the back surface.

These detector configurations provides superior resolution and the fast, uniform pulse rise time necessary for fast timing experiments.

COAXIAL DETECTORS: True coaxial detectors are right circular cylinders with the lithium doping over the entire cylindrical surface; contacts are provided at both ends. The drifted region extends from the cylindrical surface toward the center of the device. Both this sensitive region and the undrifted "p" type core of the device are symmetric with the surface along the entire length of the detector. This truly coaxial geometry retains the uniform fields and fast, uniform pulse rise times of the planar devices while providing a larger sensitive volume and therefore greater efficiency.

I.4 GAMMA-RAY PEAK SHAPE

The shape of the photoelectric peak in a Ge(Li) detector is roughly Gaussian with a low energy exponential tail[3] due to incomplete charge collection within the detector. Charge collection efficiency can be improved by increasing the detector bias. Another factor which affects the peak shape is the counting rate. In general, high counting

rate gives rise to poorer resolution. For more accurate work, it is desirable to make least square fits to the peak shapes by numerical means. A wide variety of methods and functions for peak shapes are available[4],[5],[6],[7]. In the present work, the accurate determination of intensity is not crucial, and an alternate (and simpler) method is described in the following paragraphs. It must be mentioned that the method described below is reproducible to within 3 %. Afterall, it is not the method that is of importance: it is the using of a consistent method that is of importance in the present work.

In order to calculate the intensity of a gamma-ray, we must determine the area under the photopeak. In a typical gamma-ray spectrum a variety of intensities appear ranging from very weak (a few hundred counts above background) to extremely strong ($\geq 10^4$ counts above background). For a peak sitting on a large Compton distribution, the accepted background level is a smooth line joining the Compton distribution on the low energy side of the photopeak with that on the high energy side. For the other peaks we select 10 points in front of, and 10 points behind the photopeak. The product of their average and the number of channels under the photopeak is subtracted as the background for the peak. For peaks that are closer together less points are chosen accordingly. Through-

out the course of this work, we had not encountered doublets or complex peak structures.

I.5 EFFICIENCY CALIBRATION AND ENERGY MEASUREMENTS

Before quantitative data on the relative intensities of gamma rays can be obtained from a gamma-ray spectrum, the detection efficiency of the detector must be known[8].

General noise contributions from the detector, which arises from a number of sources such as surface leakage currents and generation-recombination noise result in increased electronic noise in the system, and this increase is essentially independent of the energy of the gamma or X-rays to be detected.

The efficiency may be determined in a very simple way in the laboratory. Standard point sources of known strength are put in front of the detector at fixed geometry. In this laboratory, the distances employed are usually 1,2,6,12 and 25 cm. The number of counts of a photopeak of a given energy E is compared to the actual number of photons emitted for the same photopeak, and their ratio is defined to be the efficiency $\epsilon(E)$ at the energy E of the peak, at the particular geometry. The efficiencies at different energies at the same geometry are then plotted as a function of energy. A typical efficiency curve so obtained is shown in Figure I-4.

It was found that the efficiency curves of Ge(Li) detectors

Figure I-4

Absolute Efficiency Curve

ABSOLUTE EFFICIENCY

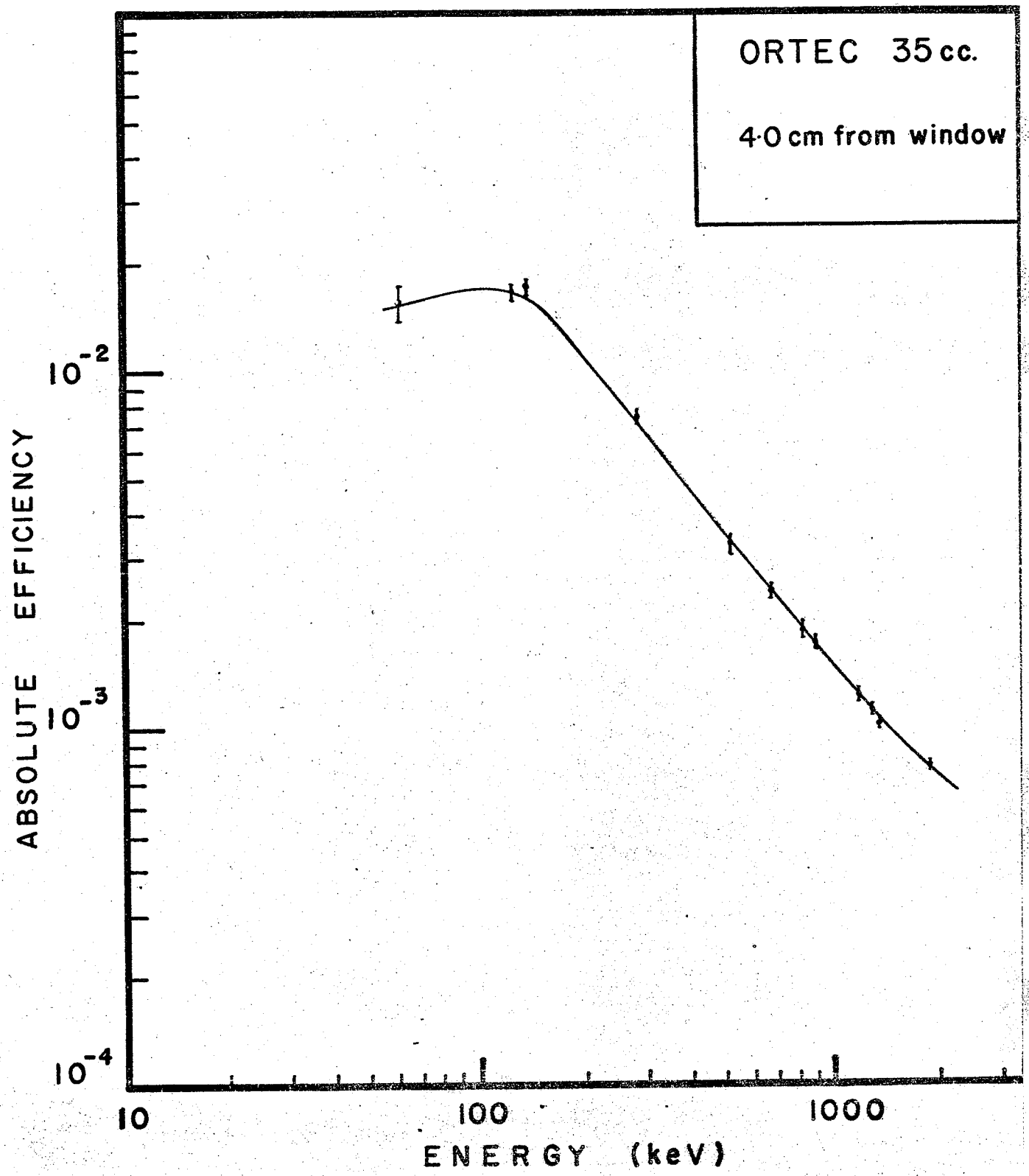

have approximately the same shape. The sources used for calibration is a set of I.A.E.A. standard sources whose activities are known. Table I-2 listed the relevant data for this set of sources.

Once this efficiency curve is constructed, efficiencies at other energies can easily be interpolated. From such a curve, it is an easy matter to obtain the absolute intensities of the gamma-rays of the isotope of interest, by putting it in front of the calibrated detector at the same (or almost the same) geometry. Suppose for a particular photopeak at energy E keV, we obtained N counts under the peak. Then the absolute intensity I(E) would be

$$I(E) = N/\epsilon(E)$$

where $\epsilon(E)$ is the efficiency at E keV as obtained from the efficiency curve. All the detectors used throughout this work had been absolutely calibrated in terms of efficiency this way.

Perhaps it is appropiate here to mention a few words about energy calibration. The energy conversion factor (that is, the number of keV per channel) depends on a number of factors, such as amplifier gain, counting rate, number of channels used, etc., so that it is impossible to obtain a calibration curve for the detector efficiency. As a matter of fact, the conversion factor changes from run to run, and sometimes, it is necessary to make an

Table I-2

I.A.E.A. Standard Sources

Nuclide	Activity μc	% Error	Half-Life	Photon Energy (keV)	%per disintegration	Total Error
^{241}Am	10.35	±0.6	432.9±0.8 y.	59.543±0.015	35.9±0.6	1.67 %
^{57}Co	11.13	0.9	271.6±0.5 d.	121.97±0.03	85.0±1.7	2 %
				136.33±0.03	11.4±1.3	11.4 %
^{203}Hg	21.02	1.0	46.57±0.03 d.	72.873±0.001	9.7±0.5	5.15 %
				82.5±0.2	2.8±0.2	7.14 %
				279.191±0.008	81.55±0.15	0.187 %
^{22}Na	9.98	0.9	2.602±0.005y.	511.006±0.002	179.7±0.8	0.445 %
				1274.55±0.04	99.95±0.02	0.02 %
^{137}Cs	11.04	1.3	30.6±0.4 y.	32.1±0.1	5.7±0.2	3.5 %
				36.5±0.1	1.3±0.1	7.7 %
				661.635±0.07	85.1±0.4	0.47 %
^{54}Mn	11.09	0.7	312.6±0.3 d.	834.81±0.03	100.00	0 %
^{60}Co	11.13	0.6	5.264±0.005y.	1173.23±0.04	99.74±0.05	0.05 %
				1332.49±0.05	99.85±0.03	0.03 %
^{88}Y	10.75	0.9	107.4±0.8 d.	898.04±0.04	91.4±0.7	0.77 %
				1836.13±0.04	99.4±0.1	0.100 %
				2734.17±0.08	0.062±0.04	6.45 %

energy calibration for each run.

It is known that when a photon enters a detector, it loses energy by creating electron-hole pairs at the rate of 2.9 eV per electron-hole pair for germanium. This rate of charge carrier pair formation is found to be nearly independent of the incident photon energy over a wide range of energies. Hence, one can assume the detector response to be approximately linear, under optimum conditions. The practical way to carry out energy calibration is to introduce standard sources of gamma-rays whose energies accurately known, and count with the source of interest. Provided that the gamma-rays do not overlap with those from the standard sources, their energies can be inferred by linear interpolation. For accurate work, one has to take into account, the non-linearity of the analyser and sometimes a polynomial fit is desirable. But for the present work, only the linear relation was used as accurate energy determination of the gamma-rays were not required. The method used to locate the centers of the peaks is a well accepted one: after subtracting background, the mid-point at F.W.H.M. was taken as the center of the peak.

I.6 REFERENCES, CHAPTER I

1) E.M. Pell, J.Appl.Phys. 31 , 291 (1960).

2) D.V. Freck and J. Wakefield, Nature 93 , 669 (1962).

3) J.T. Routti, U.C.R.L. Report#19452

4) M.A. Mariscott, Nucl.Instr. and Methods 50 , 309 (1967).

5) F.G.P. Huang and C.H. Osman,
Nucl. Instr. and Methods 68 , 141 (1969).

6) V. Barnes, United Kingdom Atomic Energy Cumberland, England.

7) J.T. Routti and S.G. Prussan,
Nucl. Instr. and Methods 72 , 125 (1969).

8) T. Paradellis and S. Hontzeas,
Nucl. Instr. and Methods 73 , 210 (1969).

9) R.A.Brown, Ph.D. Thesis, University of Manitoba, (1968).

Inner Bremsstrahlung Studies of ^{113}Sn

CHAPTER II

INNER BREMSSTRAHLUNG STUDIES OF ^{113}Sn

II.1 INTRODUCTION

The study of ^{113}In following the decay of ^{113}Sn has always been an interesting one, considering the wide range of values reported for the transition energies by different authors using different methods. Some of these values differ from others by as much of a factor of three. It is in the light of hoping to resolve this discrepancy that this work was originally initiated by late Dr.K.I.Roulston in 1964. His first attempt using NaI and 20cc germanium detector proved unsuccesful(1). The source he used had a large percentage of ^{125}Sb as a contaminant. The antimony K X-rays and tin X-rays are very close together, and the resolution of the NaI crystal was not good enough to resolve them. The impurities completely masked the inner bremsstrahlung spectrum, rendering the experiment inconclusive. This work was abandoned and resumed again in 1969, when high resolution X-ray detector and Ge(Li) detectors of high efficiency became available.

Figure II-1 shows a presently accepted decay scheme(2) of ^{113}Sn. ^{113}Sn decays to ^{113}In by electron capture with a half-life of 115 days. The electron capture branching ratio

Figure II-1

Decay Scheme of ^{113}Sn

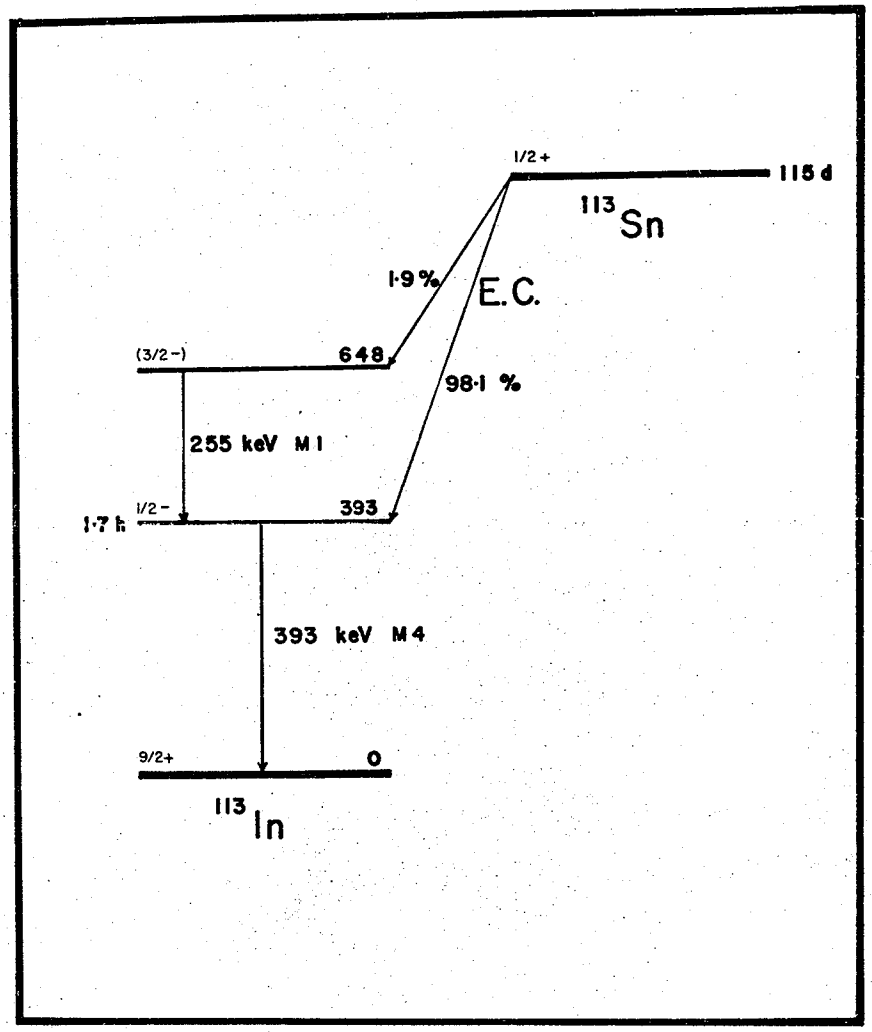
1/2+
115 d
113 Sn
1·9 %
E.C.
(3/2−)
648
98·1 %
255 keV M1
1·7 h
1/2−
393
393 keV M4
9/2+
0
113 In

to the first and second excited states are 98.2 and 1.9 to 100 respectively. The object of this work is to determine the transition energy by measuring the inner bremsstrahlung end-point energy. Once the end-point energy is known, the ground state to ground state transition energy can be obtained by adding to it 393 keV and the K-shell binding energy (28 keV).

A brief discussion of the theory involved is presented in the next section.

II.2 THEORY OF INTERNAL BREMSSTRAHLUNG DUE TO ELECTRON CAPTURE PROCESS:

In an electron capture process, the parent nucleus ${}_{z}M$ captures one of its own orbital electron, very often from the K-shell, and emits a neutrino. The final daughter nucleus has charge Z-1, and mass ${}_{z-1}M$, after the emission of any gamma ray accompanying the transition. The process can be represented by the energy equation:

$$ {}_{z}M + m_o = {}_{z-1}M + \nu + T_\nu + T_M + T_\gamma + E_K $$

where

m_o is the electron rest mass,

T_ν, T_M are the kinetic energies of the neutrino and the daughter nucleus,

T_γ is the energy of the gamma-ray(s) emitted,

E_k is the electron K-shell binding energy.

In general, $T_\nu \gg T_M$, and hence T_M can be ignored. Although T_γ is easily observable in experiment, T_ν can not be directly measured. For this reason, the transition energy has to be determined indirectly by other methods.

The best chance of electron capture by the nucleus arises from the atomic electrons spending long times in the neighbourhood of the nucleus, usually electrons from K-shell. The capture process usually leaves the daughter nucleus in the excited state, and mono-energetic gamma-rays are emitted[3]. Also, the capture of an orbital electron produces a vacancy, and an electron from the other shells may fall to fill up this vacancy, thereby producing X-rays. Auger electrons may also be produced. A further inhomogeneous non-monoenergetic gamma radiation is also produced. This is the inner bremsstrahlung caused by the changing of dipole moment of the atom when the electronic charge is suddenly changed in the capture process. For this reason, it is very logical to study inner bremsstrahlung in coincidence with the K X-rays.

Detail calculation on inner bremsstrahlung spectrum had been done by Chang and Falkoff[4], and Malasky[5]. In ground state to ground state electron capture process, the upper energy limit W_o (end-point energy) is given by the sum of the transition energy ΔE and the energy of the captured electron.

Mathematically,

$$W_o = \Delta E + m_o - E_K$$

$$= {}_zM - {}_{z-1}M - E_K$$

$$= Q - E_K$$

This implies that

$$Q = W_o + E_K \qquad \text{(II-1)}.$$

Here,

ΔE is the transition energy in nuclear mass units, and is equal to the difference of masses between the isobaric nuclei,

Q is the ground state to ground state transition energy of the electron capture process, and is usually called the Q value of the reaction.

In the present case, 98% of the electron capture decay goes to the first excited state at 393 keV, which cascades to the ground state by gamma emission.

Hence, equation(II-1) becomes

$$Q = W_o + E_K + 393 \text{ (keV)}.$$

Hence, by measuring W_o, the inner bremsstrahlung end-point energy (or simply end-point energy), we can determine the ground state to ground state transition energy Q for the electron capture process from ^{113}Sn to ^{113}In. In our case, E_K has a value of 28 keV.

In accordance with the calculations done by Schiff[6]

and Jauch[7], the energy distribution of the bremsstrahlung spectrum from electron capture process for allowed transitions is given by:

$$N(k)dk = \frac{\alpha}{\pi m_o^2 c^4} c(k) \frac{k}{W_o^2} (W_o - k)^2 dk \qquad \text{(II-2)}.$$

where

$N(k)$ is the number of inner bremsstrahlung photons with energy in the interval between k and k+dk,

W_o is the upper limit of photon energy (end-point energy)

$c(k)$ is a slow varying function in k, except at very low energies, and

k is the energy of the photon.

In ^{113}Sn study, the region of interest is greater than 500 keV, and for the present purpose, c(k) may be considered to be constant C. Hence, equation (II-2) may be rewritten as:

$$N(k)dk = K^2 . \frac{k}{W_o^2} (W_o - k)^2 dk \qquad \text{(II-3)}.$$

where

$$K^2 = \frac{\alpha c(k)}{\pi m_o^2 c^4}$$

In this experiment, N(k) and k are known quantities, as they are directly obtainable from experimental measurements. From equation(II-3) a plot of $\left[N(k)/k\right]^{1/2}$ versus k, gives a straight line with negative slope equal to $-K/W_o$, the intercept being K. Hence, the negative ratio of the intercept

and the slope should give us W_o (inner bremsstrahlung end-point energy) directly. A detail discussion on the analysis of the experimental data will be given in a later section. Such a plot resembles Kurie plot in beta work, and shall be referred to subsequently as 'Kurie type plot', to distinguish it from the genuine Kurie plot.

II.3 EXPERIMENTAL APPARATUS AND PROCEDURE

The decay of ^{113}Sn had been systematically studied, using Ge(Li) detectors. For low energy work, an Ortec X-ray spectrometer, operating at —1000 volts was used. This detector has 'chicken feed' type cryostat, and a 0.25 mm Be window. For higher energy work, (100 to 700 keV), an Ortec 35cc Ge(Li) detector was used instead. This crystal has a resolution of 2.7 keV at 1.33 MeV, and operates at a bias of +1800 volts, with a dip-stick type cryostat (See Fig. I-3). The characteristics of these detectors had been discussed in the previous chapter, and will not be repeated here.

Throughout the experiment, a Nuclear Data 2200 analyser with a 4096 channel memory was used. This instrument can be used either as a single 4096 channel analyser, or as 2 or 3 independent analysers of smaller conversion gain. For the singles gamma studies, one ADC with 2048 channels memory was found to be quite adequate. For coincidence work, a separate

time spectrum was desired. Two ADC's with 1024 channels each were used instead.

The source in the form of a chloride in 4N HCl was obtained from the New England Nuclear Corporation. The sample was 99% radiochemically pure, having a volume of 0.2 ml, and a concentration of 4.95 mc/ml. It was prepared via the reaction:

$$^{112}Sn\ (n,\gamma)\ ^{113}Sn$$

The sample was greatly enriched, and the strength was about 1 mC.

It was found that the source contained ^{125}Sb as a contaminant. Natural ^{112}Sn contains small traces of other isotopes. Neutron irradiation produces traces of active ^{125}Sn, which decays to ^{125}Sb with a half-life of 9.4 days. ^{125}Sb has a half-life of 2.7 years, as compared to the 115 days half-life of ^{113}Sn. The gamma-rays from this contaminant sit in the region where the inner bremsstrahlung photons are expected. For this reasons, it is imperative to have all traces of ^{125}Sb removed for the present work.

Figure II-2 shows a portion of singles gamma spectrum of ^{113}Sn. The first two strong lines came from ^{113}Sn. Lines at 427, 462, 598, and 604 keV can be attributed to ^{125}Sb. A separate background run was made, confirming that the lines with energies 511, 565, 583, 610, 630, and

Fihure II-2

Singles gamma spectrum with impurities

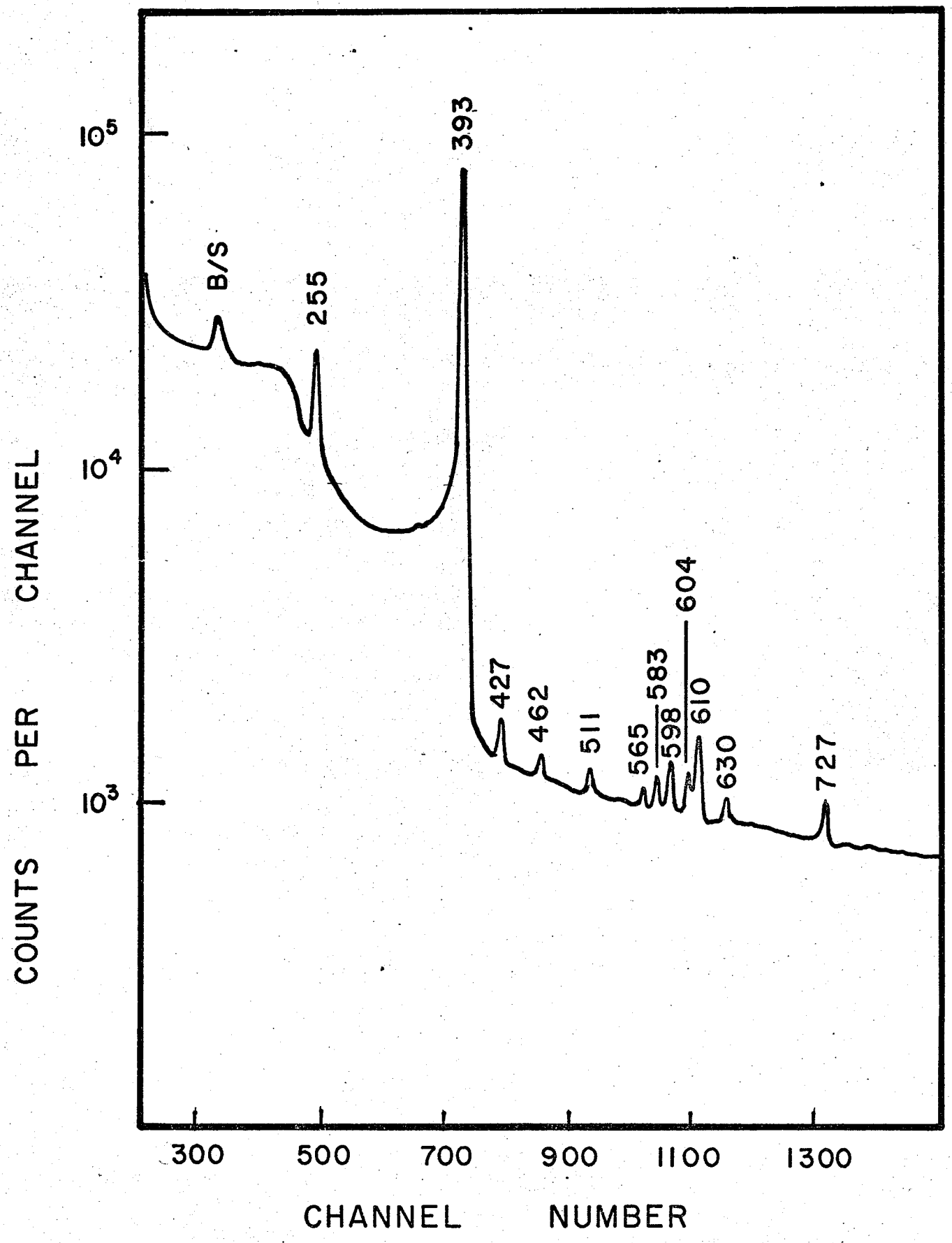
COUNTS PER CHANNEL
10^5
10^4
10^3
B/S
255
393
427
462
511
565
583
598
604
610
630
727
300
500
700
900
1100
1300
CHANNEL NUMBER

Figure II-2-A

Singles Gamma Spectrum

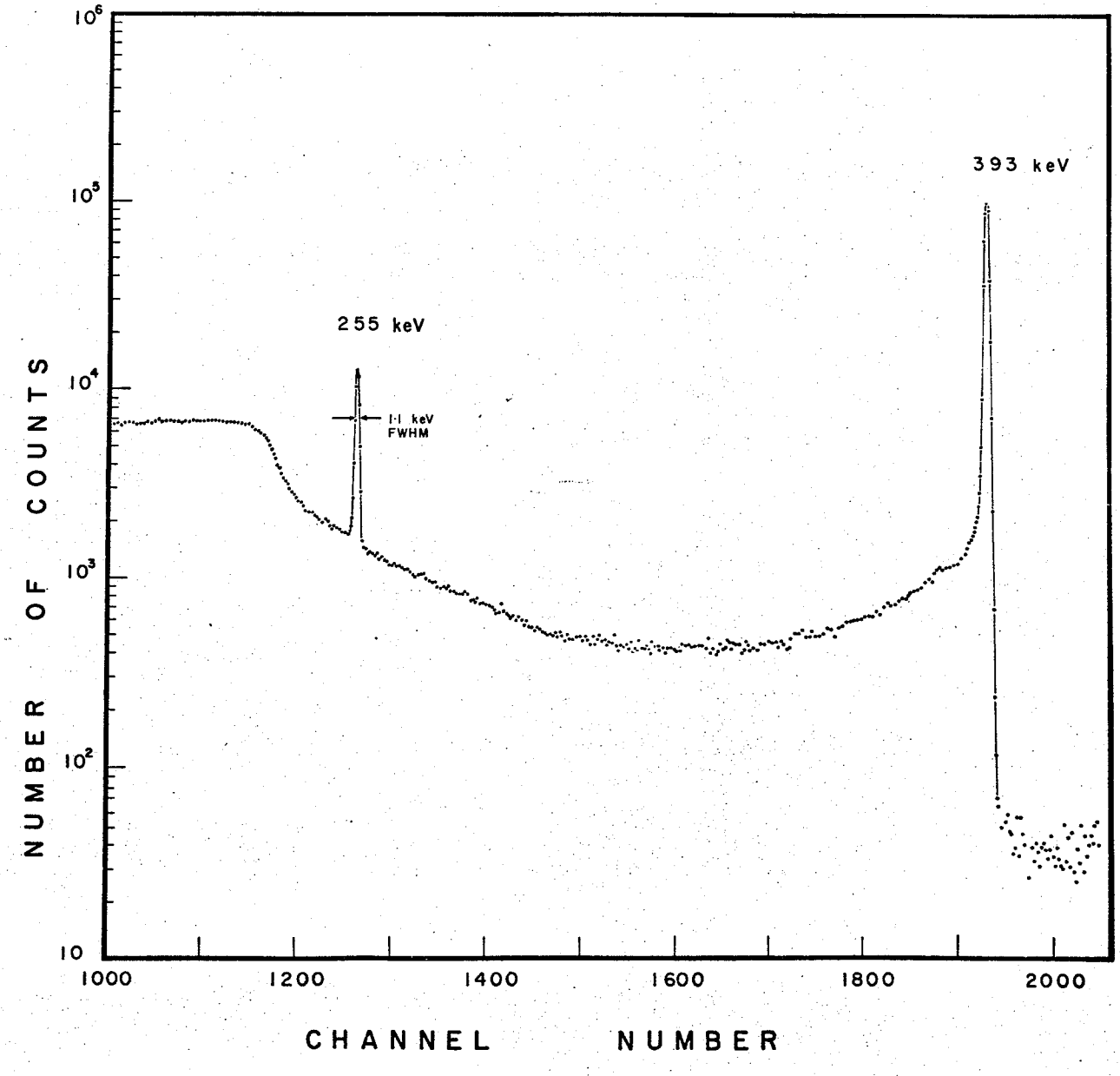
393 keV
255 keV
1·1 keV
FWHM
NUMBER OF COUNTS
CHANNEL NUMBER
10⁶
10⁵
10⁴
10³
10²
10
1000
1200
1400
1600
1800
2000

727 keV to be background contributions, from other sources in the vicinity of the detector in the same room. Subsequent runs were made which confirmed the presence of these background contributions.

In this work, the quantative presence of ^{125}Sb was obtained by comparing the intensities of the 427 keV line from ^{125}Sb, to the 255 keV line from ^{113}Sn. Before purification the ratio of the intensities of these two lines is 1.072×10^{-1} to 1. The antimony was removed chemically, and a similar spectrum was run, when the ratio was found to be 5.6×10^{-4} to 1. As a result of the purification thus the antimony concentration was effectively removed. Figure II-2-A shows a singles gamma spectrum of the purified source.

The intensity of the 255 keV line relative to the 393 keV line was determined to be $(2.9 \pm 0.3)\times10^{-2}$. For the sake of comparison, the relative intensities reported on ^{113}Sn in the literature, are listed in Table(II-1).[2],[8]→[11]

Figure II-3 shows a portion of the X-ray region. The resolution of the X-ray spectrometer is limited, so that the different X-ray components are not resolved. For example, the K_{α_2} and K_{α_1} lines are not resolved, and are indicated as a single K_{α} group. Indium K X-rays have energies 24.002, 24.2097 keV and a relative intensity of (approximately) 1:2 respectively.[21] Hence, an energy of 24.14 keV, which is the

Table II-1

The Intensity of 255 keV Gamma-Ray

Relative to 393 keV Gamma-Ray

$E(\gamma_2)$ keV	$E(\gamma_1)$ keV	$N(\gamma_2)/N(\gamma_1)$ $\times 10^{-2}$	AUTHOR
255	393	$2{\cdot}8 \pm 0{\cdot}1$	GREENWOOD and BRANNEN
257	393	$3{\cdot}0 \pm 0{\cdot}3$	GIRGIS and LIESHOUT
255	393	$2{\cdot}7 \pm 0{\cdot}2$	BURSON
255	391	$2{\cdot}9 \pm 0{\cdot}3$	BOSCH and SIMON
255	393	$2{\cdot}8 \pm 0{\cdot}3$	ROULSTON
255	393	$2{\cdot}9 \pm 0{\cdot}3$	PRESENT WORK

mean value, weighted in terms of intensities, was assigned to the K_α group. The K_β group is slightly more complicated; the strongest component occurs at about 27.3 keV ($K_{\beta_1} \sim K \rightarrow M_{III}$, 27.2759 keV). Note the presence of two peaks at 14.1 and 17.3 keV. These are germanium X-ray escape peaks[22]. They are formed when the low energy photons (here the indium X-ray photons) enter the germanium crystal, exciting the germanium X-rays which subsequently escape from the crystal. These kinds of escape peaks is common for low energy incident photons, since they interact with the germanium atoms near the front surface, and cannot penetrate too deeply into the crystal. The X-rays so produced can easily escape, giving rise to escape peaks. On the other hand, for photons of higher energies, the interactions occur deep inside the crystal. Any X-rays produced will be totally absorbed, and one would observe the full energy peaks, and no escape peaks will be apparent. At this stage, it is appropriate to point out that germanium K_α X-rays have energies very close to 10 keV, while K_β group is around 11 keV. The 14.1 keV line is the X-ray escape of the indium K_α X-ray group. Notice the presence of a small peak just at the low energy side of the escape peak, this is also an escape peak due to the escaping of the germanium K_β X-rays. Similar structure occurs for the indium K_β X-rays at 27.3 keV.

Figure II-3

Indium X-Rays.

X-RAY SPECTRUM

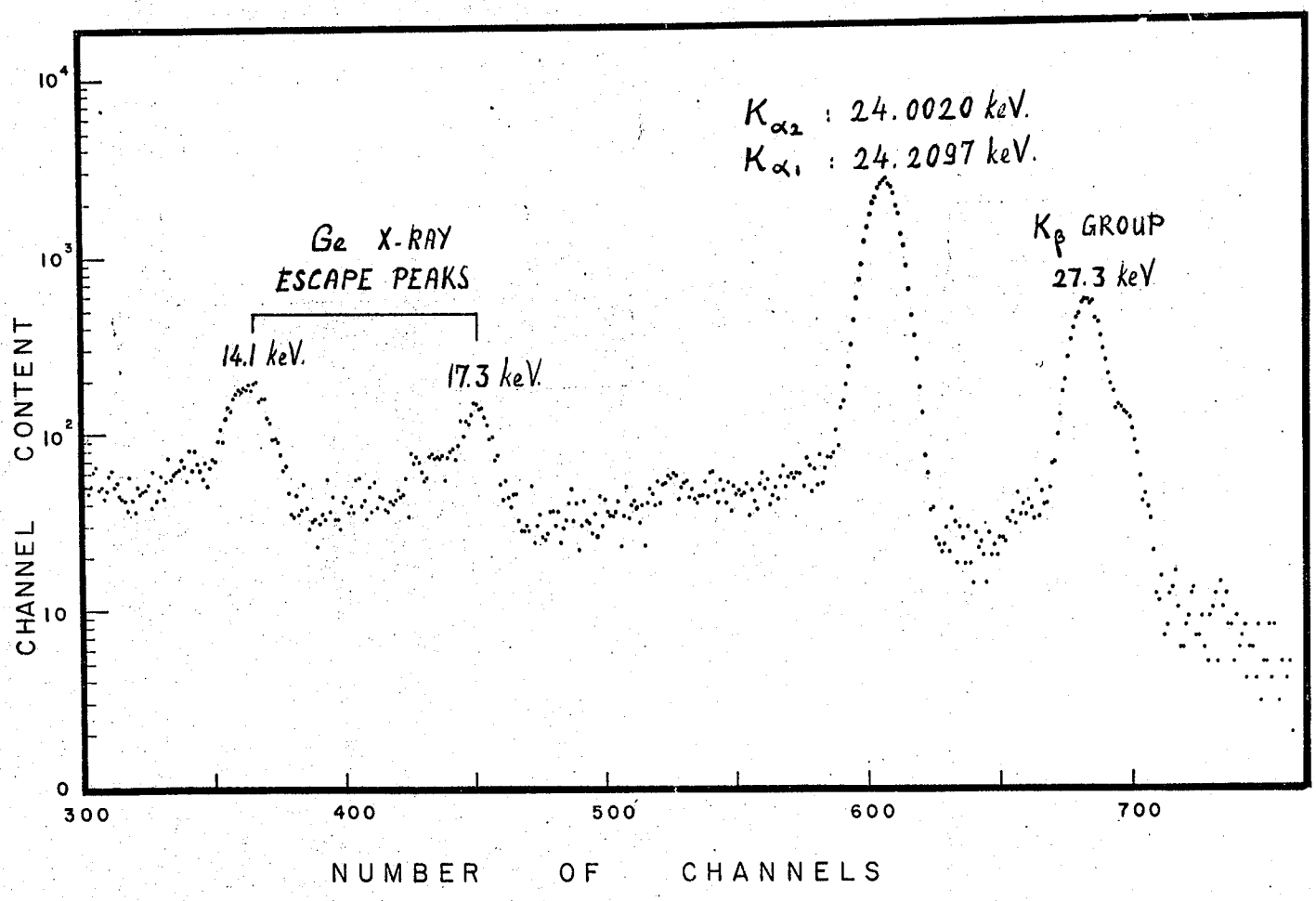

II.4 X-RAY BREMSSTRAHLUNG COINCIDENCE EXPERIMENT

In the following paragraphs, the determination of the inner bremsstrahlung end-point energy corresponding to the electron capture decay of ^{113}Sn into the first excited state of ^{113}In was discussed. As had been mentioned in the last chapter, one expects the indium K X-rays to be in true coincidence with the inner bremsstrahlung photons. Hence, a coincidence method between inner bremsstrahlung and indium X-rays was used to study the inner bremsstrahlung photons. The theoretical aspects had already been dealt with, and shall not be repeated here.

A variety of ^{113}Sn sources had been used for this work, but they were all rejected due to the presence of impurities or unsuitable strength including a cyclotron produced one. A commercially prepared one was finally obtained, purified, and was found to be very succesful. This source had a strength of approximately $\frac{1}{4}$ mC, and was dropped onto a sheet of plastic of thickness 3 mg/cm^2, and about 2 cm in diameter. It was evaporated to dryness and then covered with a second sheet of the same material. The plastic films served following three purposes:

(i) they act as backing material for radioactive source,

(ii) they cover the source so that there is greater radiation safety,

(iii) they stop, to a certain extend, some of the conversion electrons.

The source, sandwiched in plastic, was then put in a Compton shield. Figure II-4 shows a sectional view of such an arrangement. It consisted of, essentially, two lead plates of thickness 5 mm, with a hole of 1 cm diameter drilled in the centre so that the gamma-rays could reach the detectors. Such an arrangement did help to cut down compton back-scattering by the detectors[12]. However, lead X-rays might be excited, leading to spurious peaks. To cut down these X-rays, the arrangement was covered with copper plates of thickness 3 mm, with holes drilled at appropiate places. Copper is very effective in absorbing Pb X-rays (84 keV), and is easily obtainable. Also, any copper X-rays that might be produced would not be of consequence, since its energy is too low (6 to 6.8 keV) to be of any significance.

In the present coincidence work, an Ortec X-ray spectrometer was employed to gate on the indium X-rays, and an Ortec 35 cc Ge(Li) detector was used to look for inner bremsstrahlung photons in coincidence, beyond the 393 keV gamma-ray. The relative positions of the detectors and the source is shown in Figure II-5. In order to prevent any conversion electrons from entering the thin Be window of the X-ray detector, the polyethelene cover was left on throughout the experiment. This $\frac{1}{2}$ cm thick polyethelene may attenuate the X-rays a bit, but it did stop all the electrons ejected.

Figure II-4

Compton Shield.

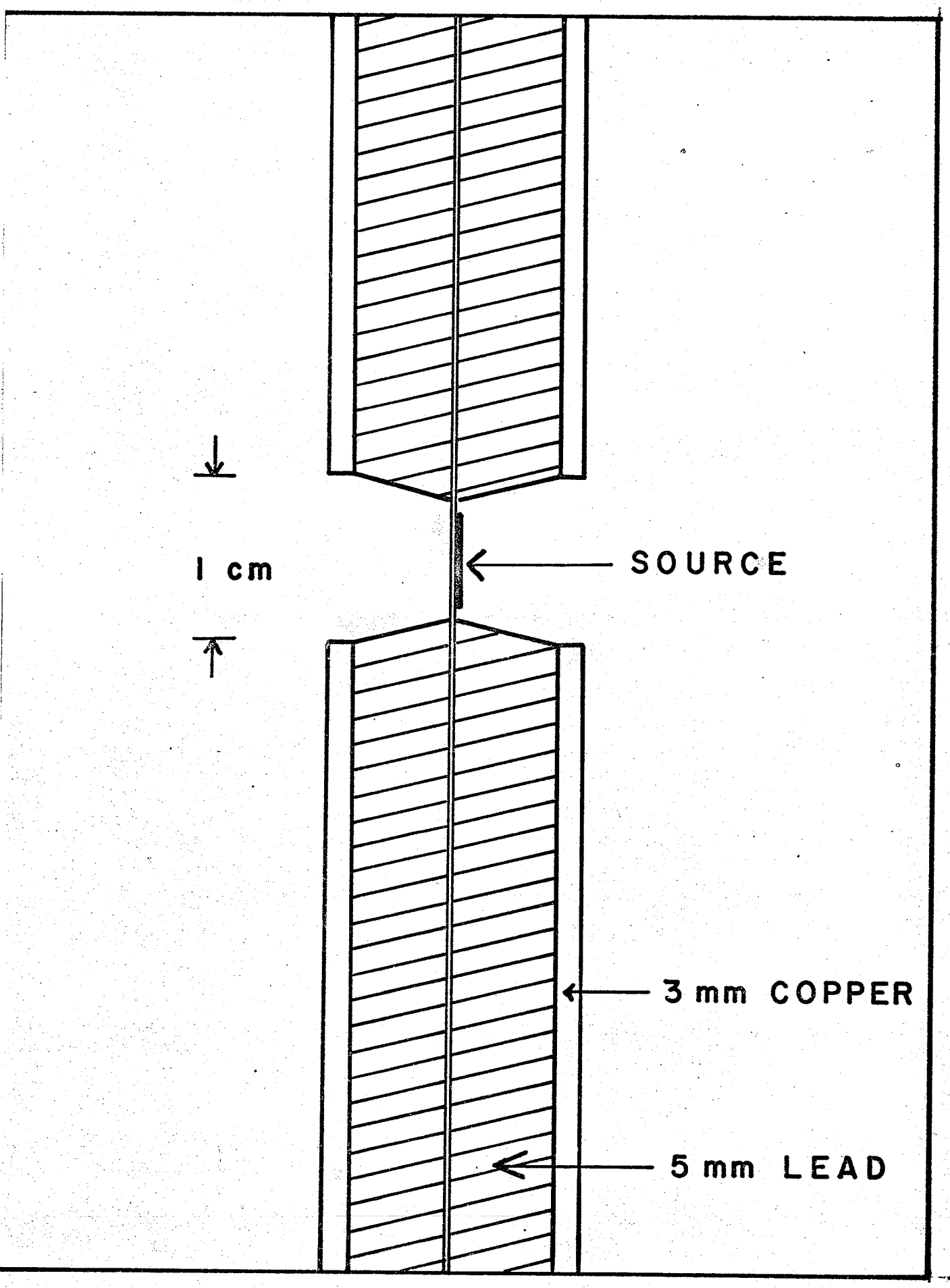
1 cm
SOURCE
3 mm COPPER
5 mm LEAD

Figure II-5

Detector Arrangement in Coincidence Experiment

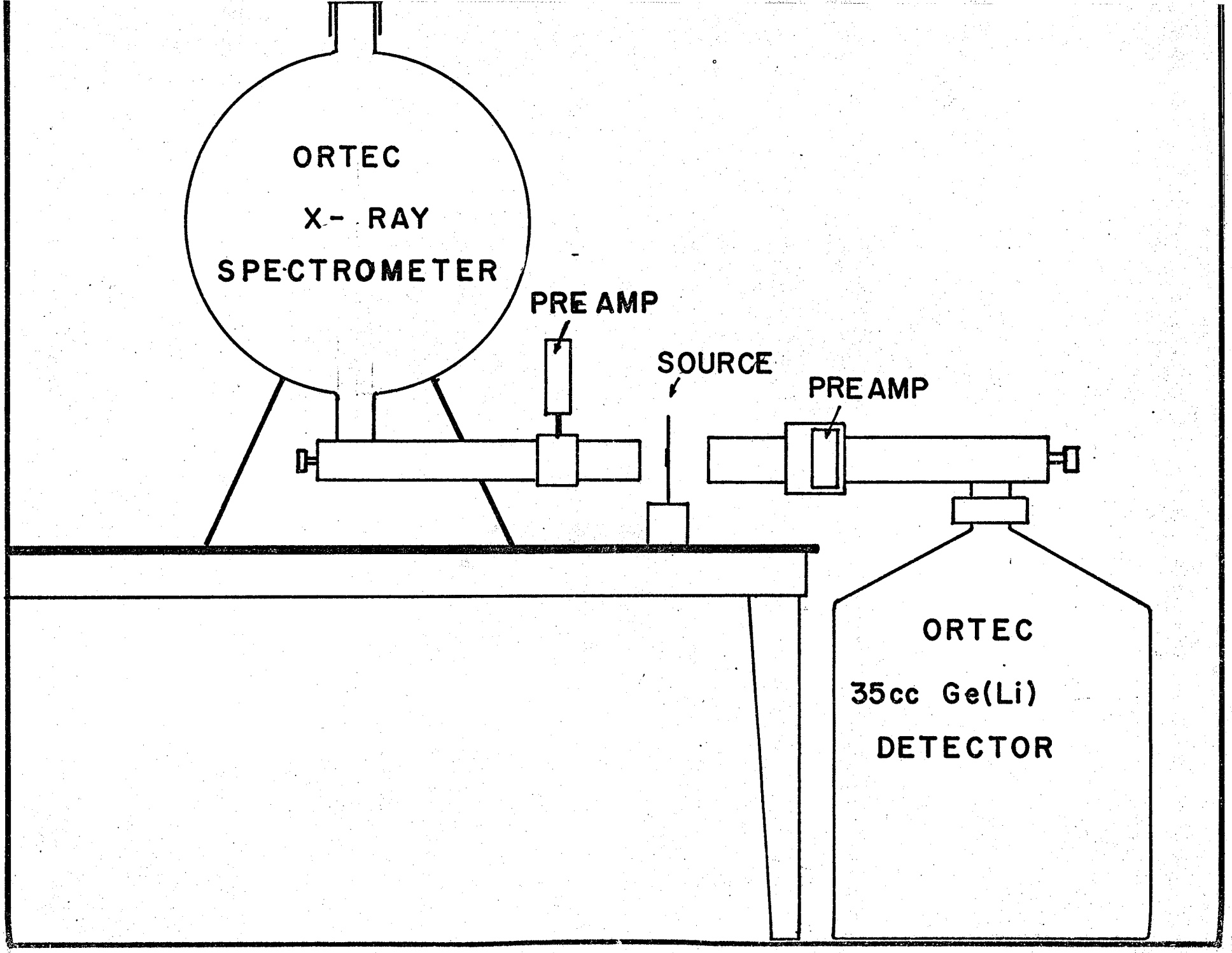
ORTEC
X- RAY
SPECTROMETER
PRE AMP
SOURCE
PRE AMP
ORTEC
35cc Ge(Li)
DETECTOR

The X-ray detector window was about 1 cm away from the source, while the 35 cc detector window was about 2 cm away. Throughout the experiment, K_α X-ray photons were used for gating, since as the K_α group is stronger, thereby giving us a better coincidence counting rate.

The coincidence circuit used was a conventional fast-slow type. A block diagram of the electronics used is shown in Figure II-6. The leading edge of the pre-amp pulses were used for fast timing. The pre-amp outputs of the two detectors were individually split into two parts. One part went into a time pick off unit (CONUCLEAR C 129A). The time pick off output, in the form of a square wave, was fed into a CONUCLEAR C 111 time analyser with the time window wide open. The other part of the pre-amp output of the X-ray detector was amplified, using a TENNELEC TC 200 amplifier, and an energy window was set on the indium K_α X-ray group, via a CONUCLEAR C 112 single channel analyser. This energy requirement was then imposed on the time spectrum from the TAC output, by using the SCA pulses to open the linear gate. A coincidence time spectrum with energy requirement is shown in Figure II-7. The range of the entire spectrum represented a time interval of 1μsec between the start and stop pulses. The time peak is narrow, with a resolution of 36 nsec. at FWHM. A time window was then set on this coincidence time peak, by means of a SCA which is built in the TAC itself.

Figure II-6

Fast-Slow Coincidence System Employing

Two Ge(Li) Detectors.

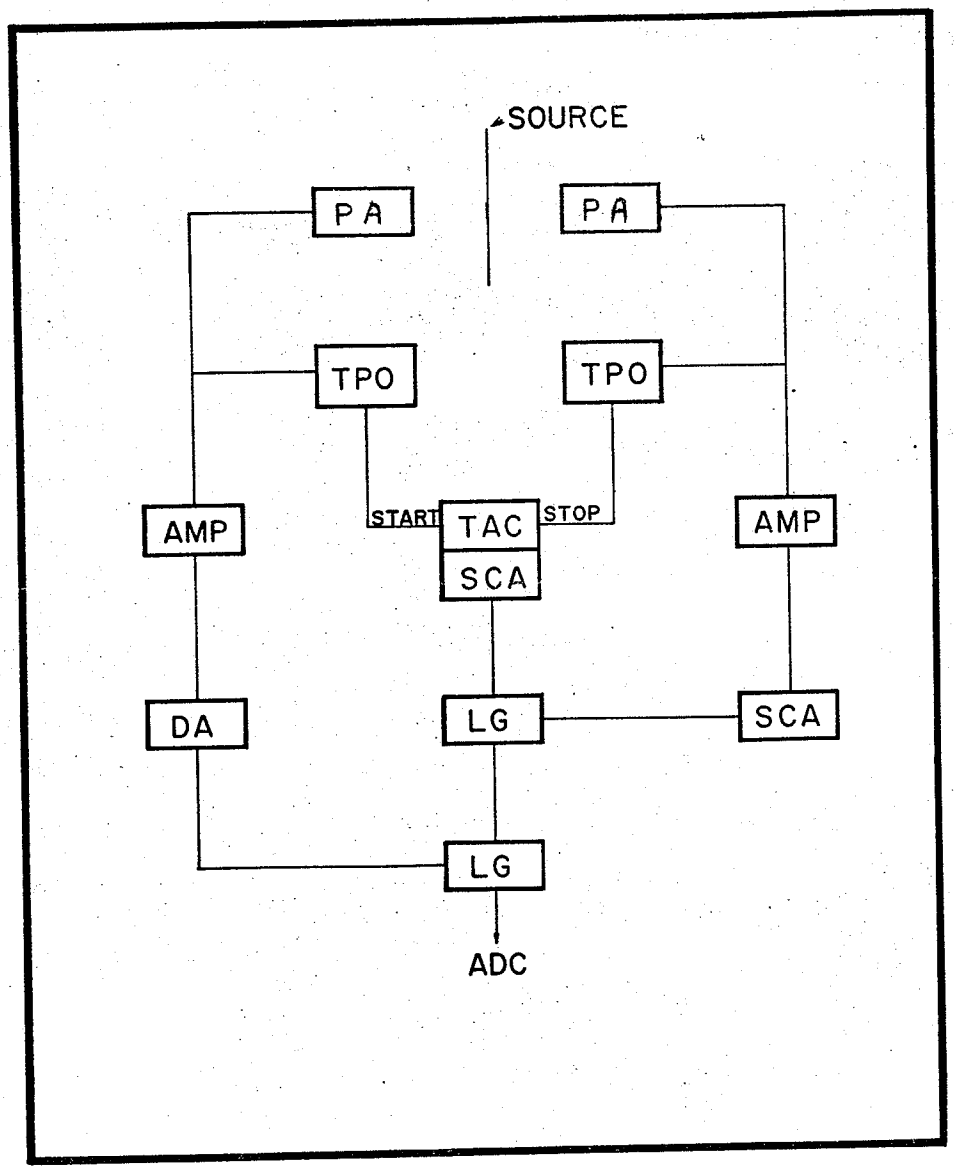
SOURCE
PA
PA
TPO
TPO
AMP
START
TAC
STOP
SCA
AMP
DA
LG
SCA
LG
ADC

Figure II-7

Coincidence Time Peak.

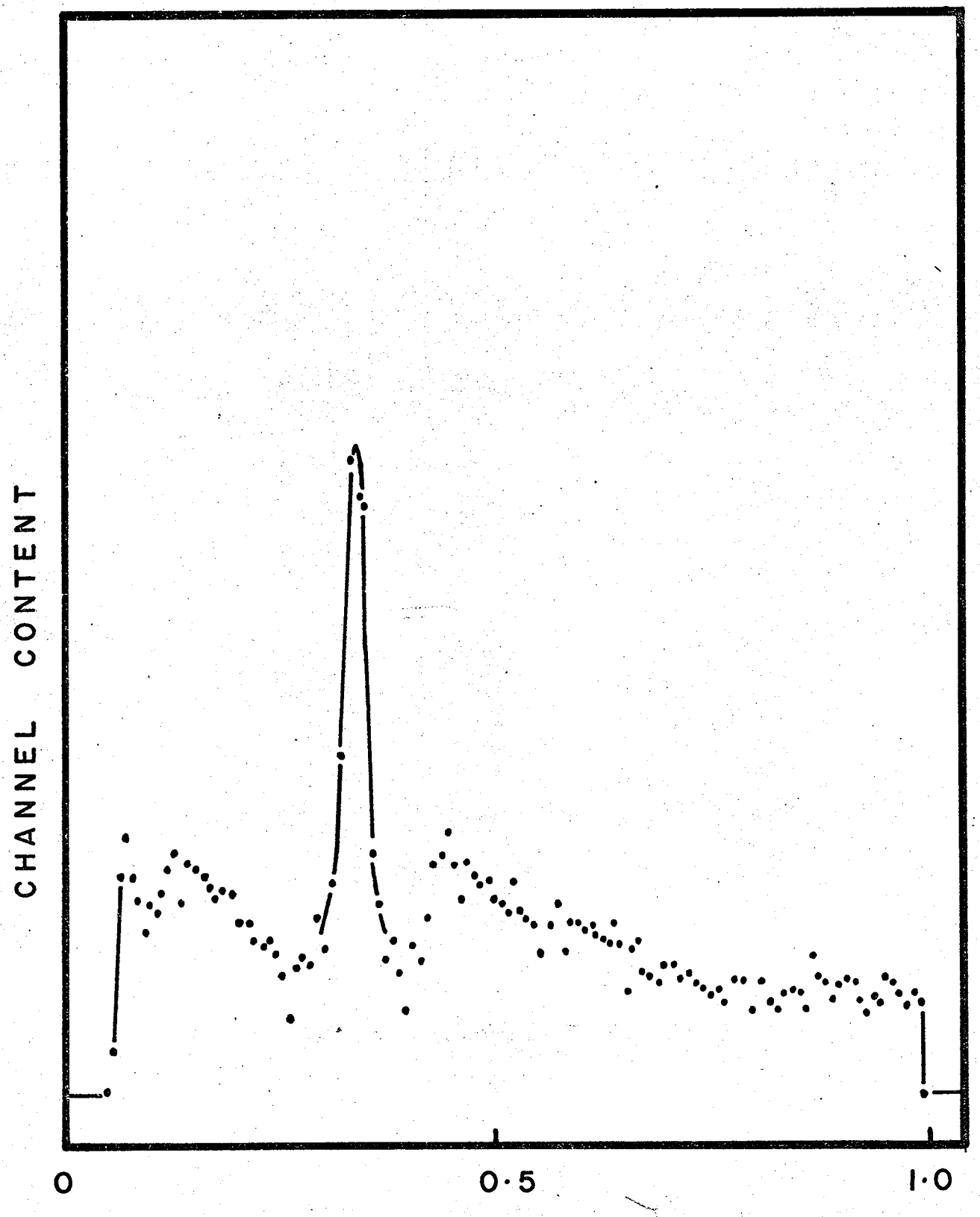
CHANNEL CONTENT
0
0·5
1·0
(TIME IN MICROSECONDS)

The pulses from the time and energy windows were then run in coincidence into a second linear gate. The other pre-amp output from the 35 cc detector was amplified (using a Nuclear ENTERPRISE NE 5230 linear amplifier) and delayed by a CO-NUCLEAR C 119 delay amplifier, and these pulses can pass through this last linear gate if and only if they are in coincidence with those from the time and energy windows. Such a circuit was found to be quite adequate for the present work.

The collection of the coincidence spectrum took a few days. The longest run attempted (and the best one) took five days. As with most coincidence work, a randoms spectrum is not only desired, but necessary. After the coincidence spectrum was collected, the energy window was shifted upwards to gate on the region just above the K_β X-ray group, with the same window width, as indicated in Figure II-8. This way, a randoms spectrum was obtained. It was found that the random counts in the region of interest was very close to a straight line, and for the subsequent analysis, a straight line background was assumed.

A portion of the coincidence spectrum is shown in Figure II-8-A. Note that the relative intensities of the 255 and 393 keV lines is reversed. This is easily understandable. If we look at the decay scheme in Figure II-1,

Figure II-8

Energy Windows for Coincidence

and Random Runs.

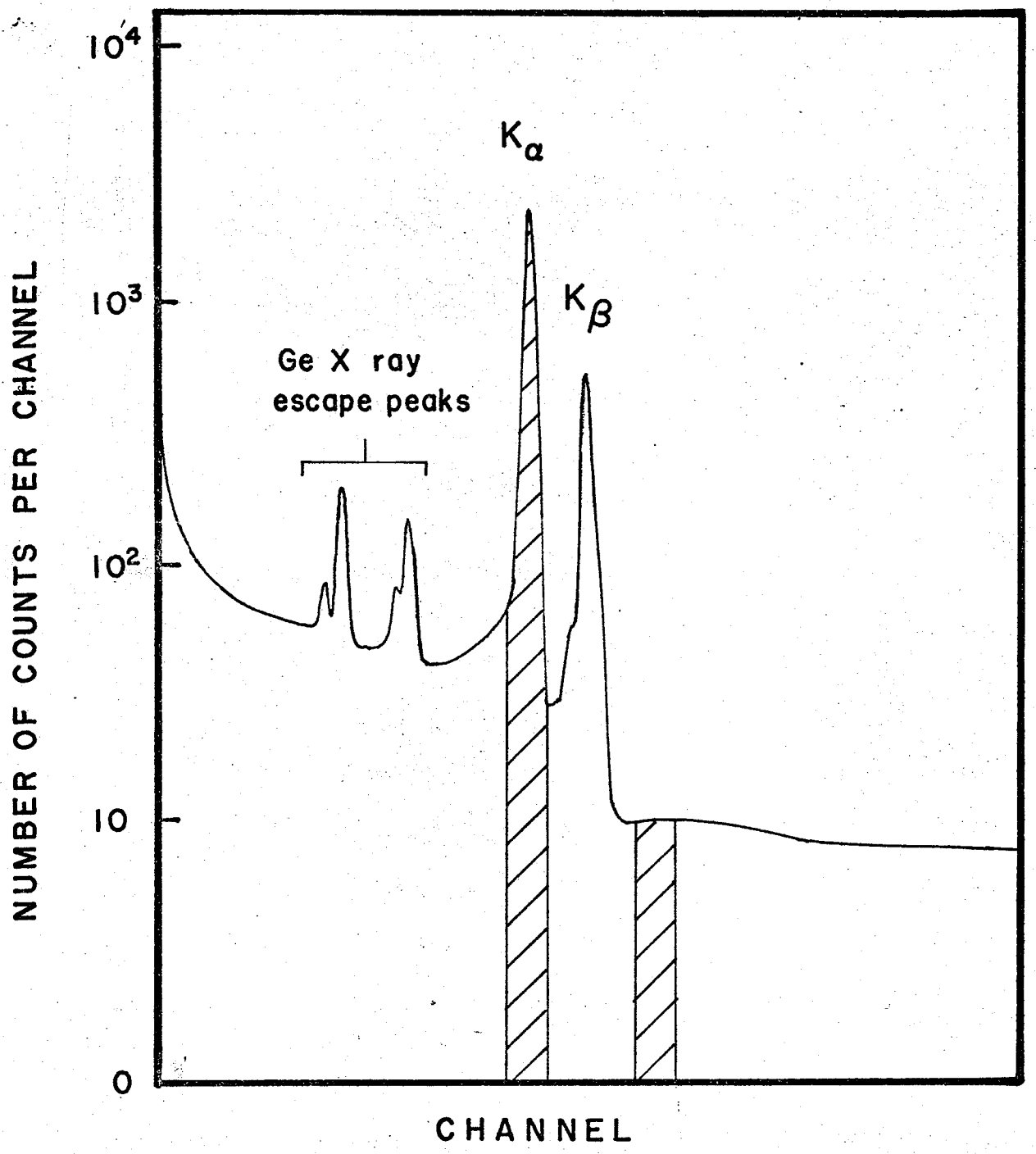
10^4
10^3
10^2
10
0
K_α
K_β
Ge X ray
escape peaks
NUMBER OF COUNTS PER CHANNEL
CHANNEL

Figure II-8-A

Coincidence Spectrum.

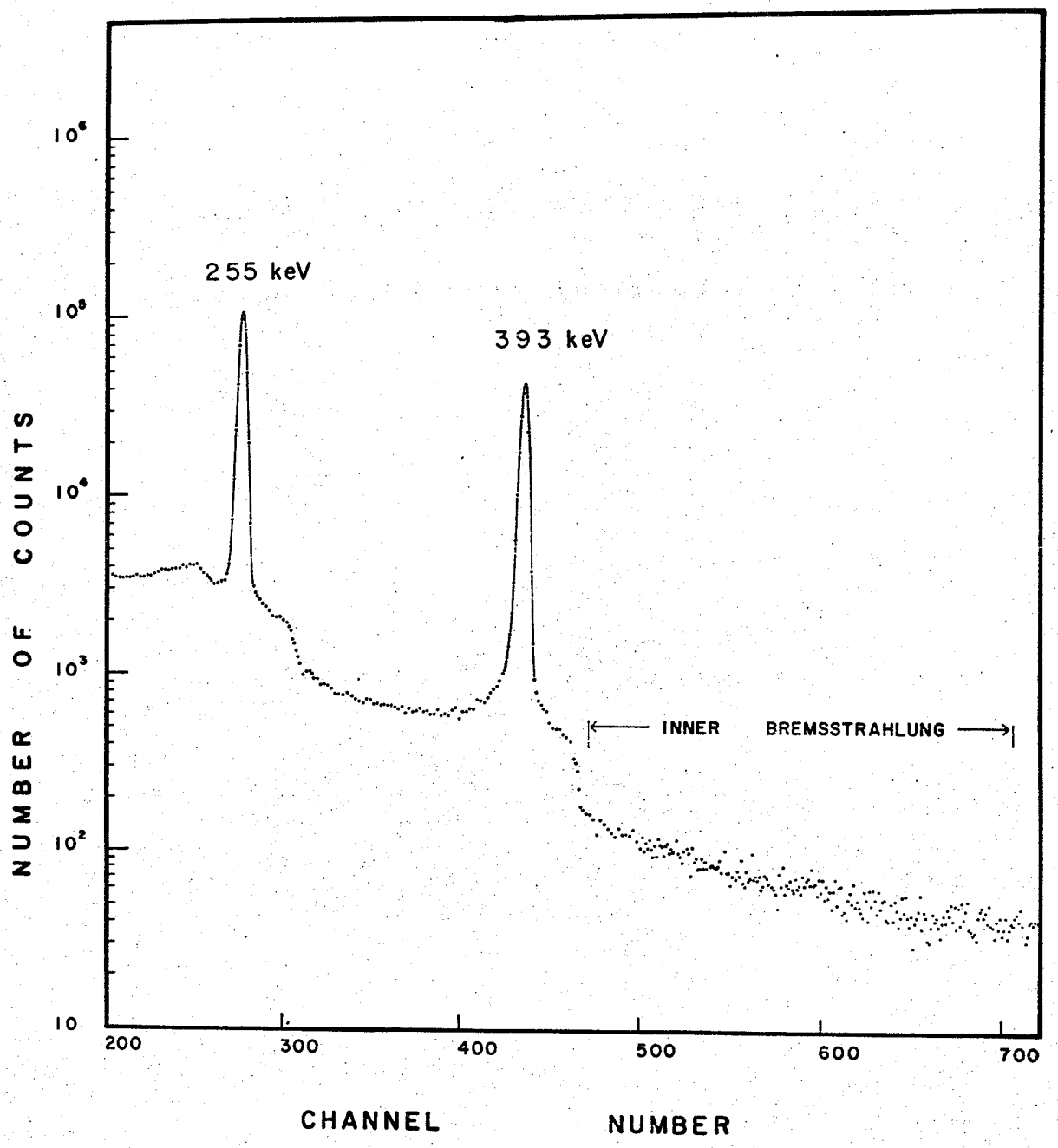
255 keV
393 keV
INNER BREMSSTRAHLUNG
NUMBER OF COUNTS
CHANNEL NUMBER
10
10²
10³
10⁴
10⁵
200
300
400
500
600
700

we see that the 255 keV line is fed by the second excited state at 648 keV, which has a half-life shorter than the time resolution of the system. This gamma-ray therefore, is in true coincidence with the indium X-rays, as we had expected. On the other hand, the 393 keV line is fed by the first excited state which long-lived, having a measurable half-life of 1.7 hours[13]. Its relatively intense presence in the coincidence spectrum due to chance coincidence may be explained by the fact that over 99% of the electron capture process decays to this level. From these intensities as well as that from the singles spectrum the true to random ratio was determined to be 30/1.

It is of interest to notice the strange structure on the high energy side of the gamma-rays. These bumps were quite puzzling, and their exact origin is not known. One very possible explanation was due to the accidental summing between the gamma-rays and indium X-rays. Since the resolution and statistics were not as good as desired, as well as the complexity of the X-ray group, the sum peaks were not resolved, but rather appeared as "bumps" in the spectrum. This explanation was deduced from energy conciderations. However, these bumps did not really affect the analysis on the inner bremsstrahlung region.

II.5 DATA ANALYSIS

At the conclusion of the run, the analyser output was first punched in paper tape, and then in cards for computer analysis. The region of interest (i.e. the inner bremsstrahlung region)was selected and the analysis was carried out by the computer automatically. In the following section the function of the computer programme will be described. A flow chart is shown in Appendix II.

First, the calibration data was read into computer. This include both energy and efficiency calibration data. For this purpose, the 255 and 393 keV lines were chosen, and their corresponding channel numbers, taken from a singles run at the same geometry shortly after coincidence and random runs. From the energy and channel difference, the energy conversion factor in keV per channel was determined. This was accomplished by simple division, since channel number was a linear function of energy. By a similar token, the efficiency at energy k can easily extrapolated, since from the efficiency curve, in the region 200 to 1000 keV, $\log_e(\text{eff})$ was approximately linear with respect to $\log_e(k)$, where eff was supposed to mean the efficiency of the detector at energy k(keV) at the particular geometry. The zeroth channel, corresponding to the channel number at 0 keV, was also calculated, and all susequent channels were corrected for this zero-cutoff

correspondingly. Next, raw data from the coincidence spectrum was read in, together with the background, which was assumed linear, and the start and stop channel number, which defined the region to be analysed (that is the inner bremsstrahlung region). The channel numbers were corrected for the zero off-set (or zero-cutoff), and converted into energy k by multiplying by the energy conversion factor. The raw data was striped off the background, and corrected for the efficiency. The new variable $z(k) = \sqrt{\frac{N(k)}{k}}$ was calculated for all points. Here, N(k) was the treated data corrected for efficiency and background. A least square fit to a straight line was made, in accordance with the equation:

$$z(k) = A.k + B$$

where A and B represented the slope and intercept of the straight line, k is the energy in keV. A theory of the least square fit is given in Appendix III. The rest of the programme was trivial, involving the calculation of the root mean square deviation, the fitted values of z(k), the end-point energy (EPE = -B/A), the ground state to ground state transition Q = EPE + 393 + 28 (keV). The output is best summarized in Figure II-9, where a Kurie type plot was shown. In this Figure, the small circles represent the experimental data. Here, $z(k) = \sqrt{\frac{N}{k}}$ rather than N were plotted versus energy k. N is the channel content corrected for efficiency, and k is the energy of the inner bremsstrahlung photons. Note that

Figure II-9

^{113}Sn Inner Bremsstrahlung Kurie Type Plot.

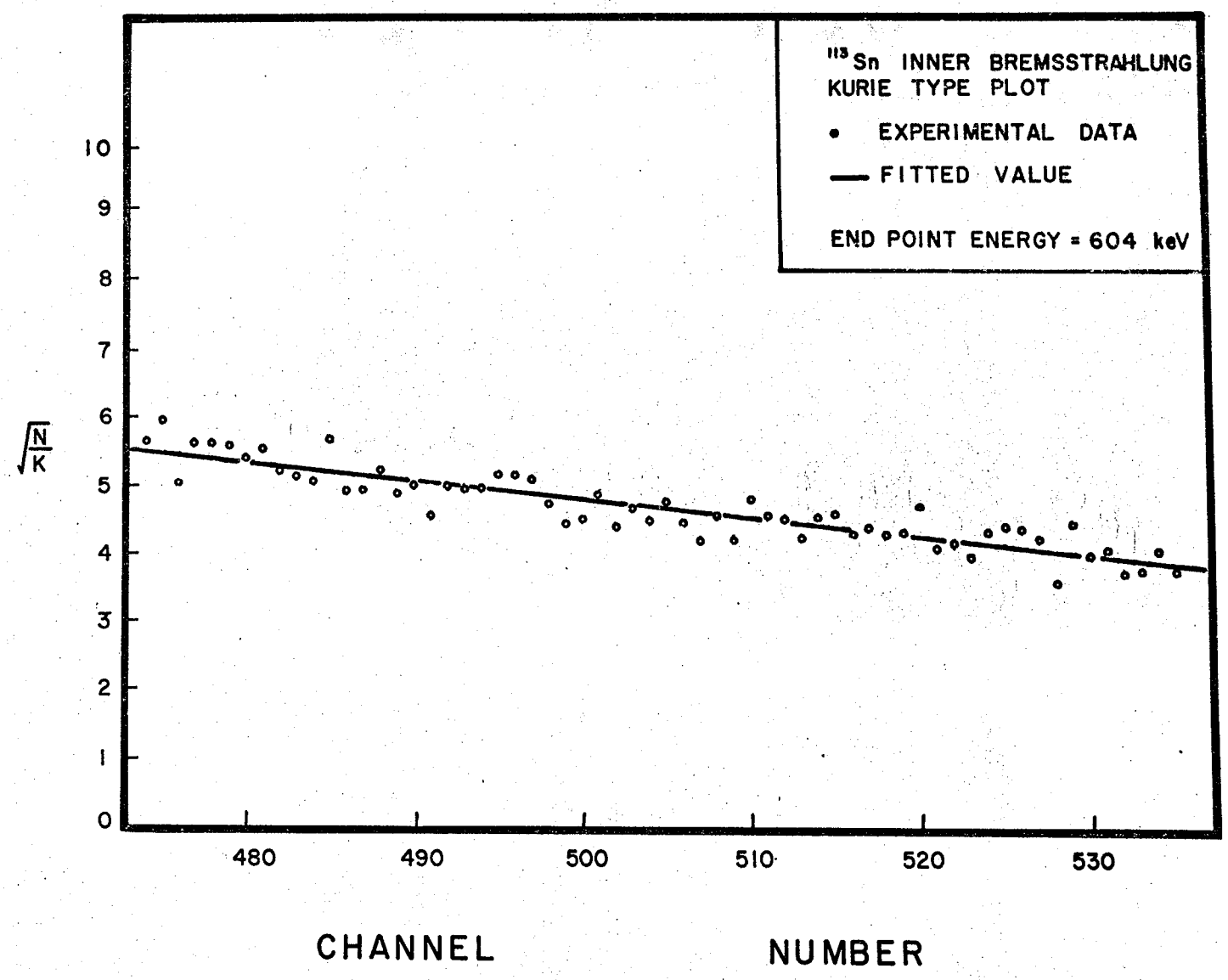
^{113}Sn INNER BREMSSTRAHLUNG
KURIE TYPE PLOT
• EXPERIMENTAL DATA
— FITTED VALUE
END POINT ENERGY = 604 keV
$\sqrt{\frac{N}{K}}$
0
1
2
3
4
5
6
7
8
9
10
480
490
500
510
520
530
CHANNEL NUMBER

the statistics were not as good as desired. On the average something like 80 counts per channel was obtained from the analyser out-put. The counting rate could have been improved by moving the detectors closer together, but this would decrease the true to random ratio. For the present run, the true to random ratio was 30:1, which was considered satisfactory. For the coincidence system, the energy resolution was 4 keV at 255 keV, as compared to 1.1 keV at the same energy in the case of singles runs.

The fitted straight line had a negative slope and positive intercept, as had been expected. Their respective values were -0.269×10^{-1}, and 0.186×10^{2}, giving us an end-point energy of 604 $\pm$ 150 keV. This is the reaction energy due to electron capture process to the first excited state of ^{113}In. From this information, the ground state to ground state transition energy was determined to be 1026 $\pm$ 150 keV.

The error involved in this experiment was estimated to be 25%. The main contribution of uncertainty comes from the relatively poor statistics as well as from the fitting procedure. Note that, from the Kurie type plot, the experimental points did not extend to the cut off channel, which was extrapolated by extending the fitted straight line until it cut the X axis corresponding to N = 0. For this reason, the uncertainty involved in the determination of the end-

point energy was high. The fitting routine calculated the root mean square deviation and this quantity was used as a test for goodness of fit as well as estimation of error. From the fitting procedure, the error was estimated to be 18.3% : this included the error due to fitting as well as statistical error. Another major source of uncertainty comes from efficiency calibration, which was usually about 7 to 10 %. Thus, the overall error was determined to be 25%. This may be considered as an upper limit of experimental error. The question of error could be a very complicated one, but it is felt that the root mean square deviation was a very reasonable estimate for this upper limit.

II.6 DISCUSSION AND CONCLUSION

In 1965, Roulston[1] estimated that the reaction Q value to be approximately 1 MeV. The present result seems to support this. Further, results reported by Cameron[14], Wapstra[15], and Phillips and Hopkins[16] are in good agreement with the present value. For the sake of comparison , the results reported, as well as methods used, are listed in Table II-2. The close agreement between our result and Wapstra's calculation may be purely coincidental, but it does reflect the fact that the true Q value to be somewhere in this neighbourhood. Sen[17] and co-workers had determined this Q value by electron-X-ray coincidence method in 1965, and their result was again in

Table II-2

Reaction Energy of Electron Capture of ^{113}Sn

AUTHOR	REACTION ENERGY TO 393keV LEVEL	Q (keV)	METHOD
Phillips[16] and Hopkins	900	1300±300	INNER BREMSSTRAHLUNG 1960
Bhatki[18]	291	702	DEDUCED FROM TRANSITION ENERGY TO 648 keV LEVEL 1957
Sen[17]	280	701^{+350}_{-150}	ELECTRON–X RAY COINCIDENCE 1965
Manduchi[19]		470	K.L X-RAY INTENSITIES 1964
Bosch[11]		760	INNER BREMSSTRAHLUNG 1967
Myers[20]		1413	UNPUBLISHED 1965
Cameron[14]		1140	UNPUBLISHED 1957
Wapstra[15]		1023	THEORETICAL 1965
Roulston[1] and Ungrin		1000	THEORETICAL ESTIMATION 1965
Present work	604	1026±150	INNER BREMSSTRAHLUNG 1970

agreement with the present work, within limits of experimental accuracy.

It is of interest to note the value reported by Bhatki[18]. Of particular interest is that reported by Manduchi[19] in 1964. His Q value obtained was 470 keV, and the method used was from K L X-ray intensities considerations. One very possible explanation for this is contamination problem. It was found that[24] for this kind of method, a trace of ^{119}Sn as a contaminant was enough to off set the Q value, by a factor of 2 or 3.

II.7 REFERENCES, CHAPTER II

1) K.I.Roulston, CAP Conference, June 1965, Vancouver.

2) C.M.Lederer, J.M.Hollander, and I.Perlman,
Table of Isotopes, Sixth Edition, John Wiley.

3) A.Snell, and F.Pleaston, Phys.Rev. 100, 1396 (1955).

4) C.S.W.Chang, and D.L.Falkoff, Phys.Rev. 76, 365 (1949).

5) Madensky, Phys.Rev. 84, 596 (1951).

6) L.Schiff, and P.Morris, Phys.Rev. 58, 24 (1940).

7) J.Jauch, O.R.N.L. 1102.

8) R.C.Greenwood, and E.Brennen, Phys.Rev. 122, 1849 (1961).

9) R.K.Girgis, and R.van Lieshout, Physica 24, 672 (1958).

10) Burson, Grench, and Schmud, Phys.Rev. 115, 188 (1959).

11) H.E.Bosch, and M.C.Simon, Phys.Rev. 159, 1029 (1967).

12) M.J.Canty, Private Communication, (1969).

13) J.L.Lawson, and J.W.Cork, Phys.Rev. 57, 982 (1940).

14) A.G.W.Cameron, Chalk River Project, Report #CRP-690 (1967).

15) Wapstra, Mattauch, and Thiele, Nucl.Phys. 67, 1 (1965).

16) Phillips, and Hopkins, Phys.Rev. 119, 1315 (1960).

17) I.O.Durosinmi-Etti, D.R.Brundit, and S.K.Sen,
Proceedings of the International Conversion Process.
(Academic Press Inc., New York, 1965), p.201.

18) Bhatki, Gupta, Jha and Madan,
Nuovo Cimento, 6, 1464 (1957).

19) Manduchi, Nardelli, Russo-Manduchi, and Zannoni,
Nuovo Cimento, 31, 1380 (1964).

20) Myers, and Swiatecki, University of California, Radiation Laboratory, Report#UCRL-11980 (1965).

21) J.A.Bearden, "X-ray Wavelengths", Report#NYO-10586 (1964).

22) W.Teoh, Private Communication, (1970).

23) K.Siegbahn, "Beta and Gamma ray Spectroscopy", North-Holland Publishing Co., Amsterdam (1955).

24) L.Martin, O.R.N.L., Private Communication (1970).

Geochemical Analysis

of

Naturally Radioactive Canadian Rocks

CHAPTER III

GEOCHEMICAL ANALYSIS OF NATURALLY RADIOACTIVE CANADIAN ROCKS

III.1 INTRODUCTION

In this part, we are interested in determining the concentrations of trace elements (Uranium, Thorium, and Potassium) in rocks. Such an information is of importance to the Earth Science Department. It is known that, the distribution or re-distribution of those trace elements in rocks is, generally, governed by the nature of the original source as well as the partitioning factors involved in the magnetic and metamorphic processes. Increased solubility of the U^{6+} ion accounts for the markedly disturbed Th/U ratios in those rocks which were formed under oxidizing conditions. Otherwise, U^{4+} and Thorium tend to be geochemically similar in the sense that the relative proportion varies by a factor no greater than 3 to 4.

The purposes for undertaking this study are:

(1) To increase the understanding of the factors which govern the distribution of these trace elements, by correlating with other investigators' observations.

(2) To aid to a lesser extent to search for economically feasible amount of Uranium and Thorium.

(3) As a guide to "heat flow" studies, it provides an estimate

of mean surface radioactivity which accounts for part of the surface heat flow.

The present method provides an accurate means of measuring the concentrations of U, Th, and K. This provides an alternate method to isotope dilution mass spectroscopy.

III.2 GENERAL GEOLOGY OF THE ROCK SAMPLES

These samples have been taken from a region of the Precambian shield. They represent granitic rocks of various composition and age. There is a general predominance of granodiorite and quartz monzonite. The intrusive episodes represented by these units span a range of time from about 2.7 to 2.5 x 10^9 years. As yet, radiometric age determination have not adequately resolved individual intrusive episodes within that time range. Relative ages have been determined (not unambiguously in many cases) on the bases of structural inference (boundary relationships, etc.).

K, U, and Th IN ROCKS:

K -----contained in potassium feldspar ($KAl_3Si_3O_8$) and in mica, biotite, and muscovite otherwise as a trace constituent of other elements.

Th,U---contained in accessory minerals and situated along grain boundaries.

Zircon, sphene, and apatite are the most likely carriers of uranium. Monazite and allanite are mainly thorium carriers.

Thus the abundance and relative proportions of U, and Th is largely controlled by the distribution of these accessory minerals. Potassium generally constitutes 2 to 5% by weight of granitic rocks.

The rock samples are designated by FM. A list of the samples is shown in the following, together with their location:

FM-1(3), FM-31(1): Samples of the latest batholithic intrusions in this area. The Lac du Bonnet quartz manzonite around Lac du Bonnet (FM-31), and its counterpart (FM-1) to the south of Hwy#1.

FM-100(3) : A melanocratic porphyritic granite related to theLac du Bonnet quartz manzonite, presumably as a border phase.

FM-68(3) : A pegmatite which is interpreted as the late stage product of this latest batholith.

FM-22(2) : A gneissic granodiorite showing distinct compositional banding. Some due to near-concordant injection of pink granite veins. This unit, part of the English River gneissic belt, may have been remobilized during the latest intrusive episode.

FM-24(2) : A hornblende-diorite from the Granite Lake stock, south of the English River gneissic belt on Hwy#1.

FM-27(2) : A one foot wide aplite dyke which cuts the Granite Lake diorite.

FM-14(2) : An aplite dyke which cuts the Indian Reserve granodiorite.

III.3 NATURAL RADIOACTIVITY AND RADIOACTIVE SERIES

Measurements of the rate of decay of a radioactive substance are purely statistical averages based on measurements made with large numbers of atoms. An atom has no memory of past events. Nor does its life expectancy decrease with age, as it does with human beings. Quantum mechanics can predict the probability of decay of radioactive atoms, but it cannot tell us if the decay in a given atom is a result of favorable conditions that occur only at intervals in a way which we cannot foresee.

When the nucleus of an atom emits an alpha or beta ray, sometimes accompanied by a gamma-ray, the process is called "radioactive decay", and the product nucleus is often found also to be radioactive.

As a result of physical and chemical research on the naturally occuring radioactive elements, it was proved that each radioactive nuclide is a member of one of three long chains, or radioactive series. In each series, the parent nuclide decays into a daughter nuclide which decays in turn, and so on, until finally a stable end product is reached. (See Table III-1).

Table III-1

Uranium Series.

ELEMENT	Symbol	Half-Life	Emitted Ray
Uranium	$_{92}U^{238}$	4.5×10 yr	α
Thorium	$_{90}Th^{234}$	24 days	$\beta(\gamma)$
Protoactinium	$_{91}Pa^{234}$	1.14 min	$\beta(\gamma)$
Uranium	$_{92}U^{234}$	3×10^{5} yr	α
Thorium	$_{90}Th^{230}$	83,000 yr	$\alpha(\gamma)$
Radium	$_{88}Ra^{226}$	1,600 yr	$\alpha(\gamma)$
Emanation	$_{86}Em^{222}$	3.7 days	α
Polonium	$_{84}Po^{218}$	3.05 min	α
Lead	$_{82}Pb^{214}$	26.8 min	$\beta(\gamma)$
Bismuth	$_{83}Bi^{214}$	19.7 min	$\beta(\gamma)$
Polonium	$_{84}Po^{214}$	10^{-5} sec	$\alpha(\gamma)$
Lead	$_{82}Pb^{210}$	22 yr	β
Bismuth	$_{83}Bi^{210}$	5 days	$\beta(\gamma)$
Polonium	$_{84}Po^{210}$	140 days	α
Lead	$_{82}Pb^{206}$	Stable	

Table III-2

Thorium Series.

ELEMENT	Symbol	Half-Life	Emitted Ray
Thorium	$_{90}Th^{232}$	$1{\cdot}39\times10^{10}$ y	α
Radium	$_{88}Ra^{228}$	6·7 y	β
Actinium	$_{89}Ac^{228}$	6·13 h	β
Thorium	$_{90}Th^{228}$	1·910 y	α
Radium	$_{88}Ra^{224}$	3·64 d	α
Radon	$_{86}Rn^{220}$	51·5 s	α
Polonium	$_{84}Po^{216}$	0·16 s	α,β
Lead	$_{82}Pb^{212}$	10·6 h	β
Astatine	$_{85}At^{216}$	3×10^{-4} s	α
Bismuth	$_{83}Bi^{212}$	60·5 m	α,β
Polonium	$_{84}Po^{212}$	$3{\cdot}0\times10^{-7}$ s	α
Thallium	$_{81}Tl^{208}$	3·10 m	β
Lead	$_{82}Pb^{208}$		Stable

These series are named the Uranium, Actinium, and Thorium series respectively, after elements at, or near, the head of the series. In the Uranium series, the mass number of each member can be expressed in the form (4n+2), where n is an integer, and the Uranium series is sometimes called the '4n+2' series. In the Actinium and Thorium series, the mass numbers are given by the expressions '4n+3' and '4n' respectively. The series '4n+1' is missing in nature. It is considered probable that this series existed in the bygone ages in the earth, but has since almost decayed completely. This series has been produced artificially, but it does not concern us in the present work.

The members of Uranium and Thorium series are listed in Table III-1 and Table III-2 respectively.

III.4 EXPERIMENTAL PROCEDURE

It is well known that the contents of Uranium, Thorium and Potassium in a thick rock layer may be determined by gamma-ray spectroscopy. Detectors may be used to detect gamma-rays emitted by members belonging to the radioactive series, and these gamma rays can be used to identify the elements as well as to determine their concentrations. Table III-3 indicates the gamma-rays we are interested in, as well as their origin from which the particular element (to be more exact, the particular isotope) can be identified. Throughout the course of this work, it is implicitly assumed that the radioactive nuclides in each series are in radioactive equilibrium with each other.

Table III-3

Gamma Rays and Their Origin.

ENERGY (keV)	ORIGIN PARENT ⟶ DAUGHTER	SERIES
510	$_{81}Tl^{208} \xrightarrow{\beta^-} {}_{82}Pb^{208}$	Th
584	$_{81}Tl^{208} \xrightarrow{\beta^-} {}_{82}Pb^{208}$	Th
610	$_{83}Bi^{214} \xrightarrow{\beta^-} {}_{84}Po^{214}$	U
727	$_{83}Bi^{212} \xrightarrow{\beta^-} {}_{84}Po^{212}$	Th
860	$_{81}Tl^{210} \xrightarrow{\beta^-} {}_{82}Pb^{210}$	U
910	$_{89}Ac^{228} \xrightarrow{\beta^-} {}_{90}Th^{228}$	Th
967	$_{89}Ac^{228} \xrightarrow{\beta^-} {}_{90}Th^{228}$	Th
1460	$_{19}K^{40} \xrightarrow[E\cdot C\cdot]{\beta^+} {}_{18}Ar^{40}$	
1764	$_{83}Bi^{214} \xrightarrow{\beta^-} {}_{84}Po^{214}$	U
2614	$_{81}Tl^{208} \xrightarrow{\beta^-} {}_{82}Pb^{208}$	Th

In order to be statistically meaningful, we choose the lines that are reasonably intense. For the determination of Thorium concentration, we used the 584, and 2614 keV lines. For the case of Uranium, we used 610, and 1764 keV lines. In the case of Potassium, we have no alternative but to use the 1460 keV line, as this is the only gamma-ray emitted. In situations where more than one line was used, the concentrations were determined from each line, and the average was taken.

The gamma spectrum was investigated using solid state detectors. Two Ge(Li) detectors were used for this purpose. One is a 20cc PRINCETON GAMMA-TECH. germanium detector, the other is an ORTEC 35cc germanium detector. The characteristics of these detectors have been explained in Chapter I, and shall not be repeated here.

In terms of efficiency, these detectors are only 6% and less as efficient as a 3X3 NaI detector. For this reason, we had to use large samples. We gave up using NaI detectors on account of resolution. The samples were crushed and put in a lucite container cylindrical in shape (3" in diameter, 2.3" high) and the weight of the samples were of the order of 200 to 400 gms.

At first, it was thought that the physical form of the sample would influence our result. Experiments were

run of the same sample in chips, finely ground powder, as well as a mixture of both. The result obtained showed that the attenuation was independent of the physical form of the sample. Throughout the rest of the work, no allowance was made for the attenuation due to the walls of the containers.

A schematic diagram of the electronics is shown in Figure III-1. Everytime a photon from the sample enters the detector, a pulse is generated. This tiny pulse is amplified by the pre-amp, and then by the main amplifier. It is then fed into a multi-channel analyser. The 20cc Princeton Gamma-Tech. detector was coupled to a conventional FET pre-amp, supplied by Co-Nuclear of Winnipeg, Manitoba (Model#C-403), and a Nuclear Enterprise NE 5230 amplifier was used. For the ORTEC 35cc detector, a charge sensitive pre-amp with cooled FET first stage was used (ORTEC model#116); and a TENNELEC TC 200 amplifier was employed as the main amplifier.

The gamma spectrum was recorded with a Nuclear Data ND 2200 multichannel analyser. Usually, we found that the best result was obtained using ADC#1 with 2048 channel memory. Because of the relative inefficiency of the detectors, the counting rates were extremely low. The collecting time varied from 40 hours to 140 hours. Several steps were taken:

1) The sample was put next to the detector window to ensure as high a counting rate as possible.

Figure III-1

Typical Singles Gamma-Ray Spectrometer.

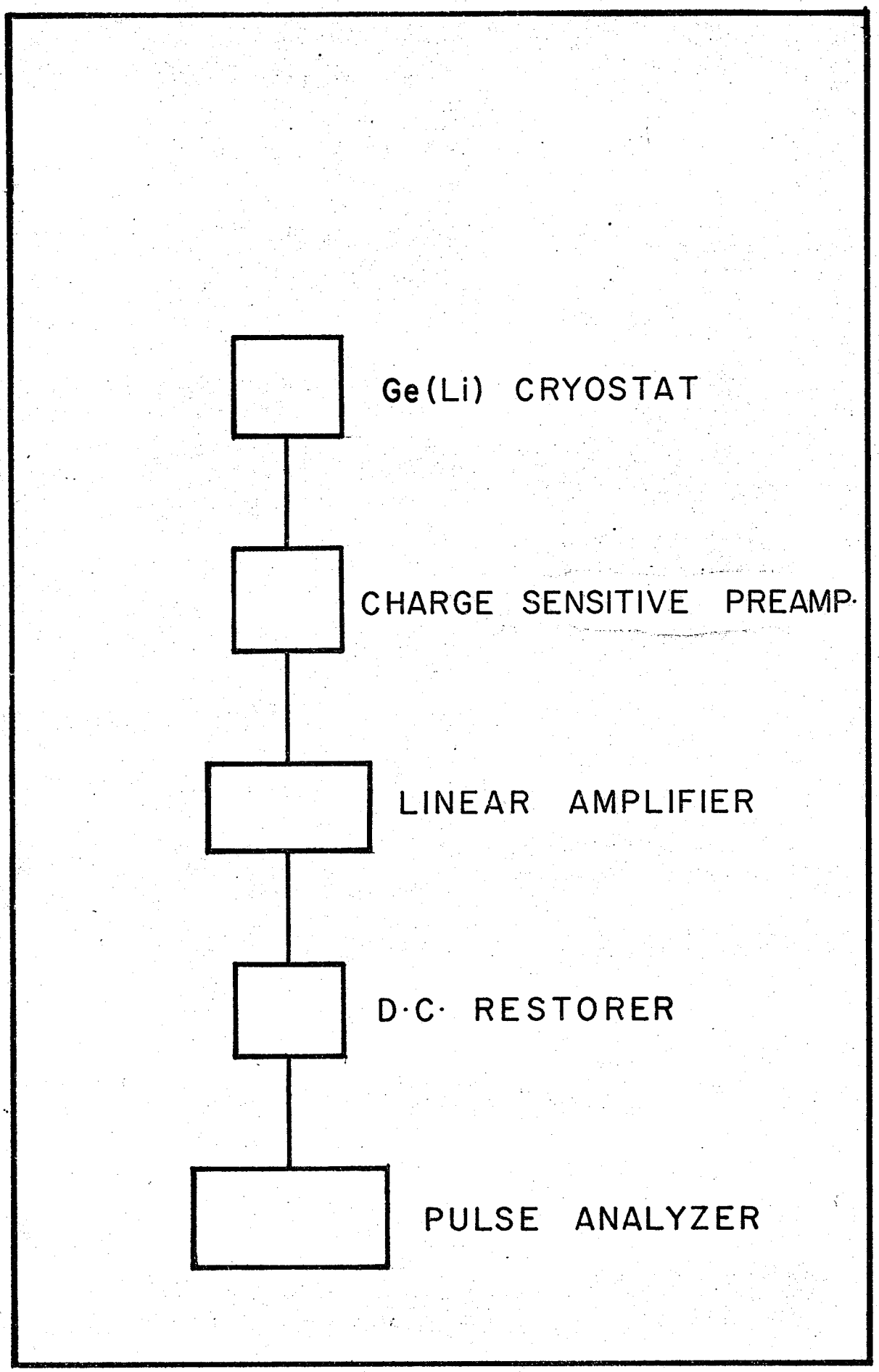
Ge(Li) CRYOSTAT
CHARGE SENSITIVE PREAMP.
LINEAR AMPLIFIER
D.C. RESTORER
PULSE ANALYZER

2) The detector and sample assembly was enclosed in a heavy lead shielding of thickness 6.5 cm. A diagram of such an assembly is shown in Figure III-2.

3) The spectrum was collected at the same time, using an arrangement as shown in Figure III-2. The outputs of the two detectors were fed into two independent amplifiers and ADC's, thereby cutting down the experimental time by a factor of two.

A typical gamma spectrum of such a rock sample is shown in Figure III-3. Notice that we see practically all the lines reported in Table III-3, except for the 727 and 860 keV lines since they are too weak to be of any statistical significance. In addition, we see peaks at 662, 1173, 1333 keV. These are attributed to background, and were believed to have come from ^{137}Cs, and ^{60}Co respectively. Also, part of the 1460 keV line from ^{40}K comes from background, as we shall see in the following paragraph.

To determine the concentration of the trace elements, a similar spectrum was run, using a standard source composed of known amounts of each Uranium, Thorium and Potassium, at the same geometry. All the photopeaks are normalised to 100 hours collecting time. The ratio of the areas of the corresponding peaks gives the ratio of the concentration of the corresponding trace elements. In this way, the detection efficiency of the detectors as well as the attenuation was eliminated. A slight complication arose for the case of potassium peak at 1460 keV.

Figure III-2

Arrangement of Source and Ge(Li) Detectors.

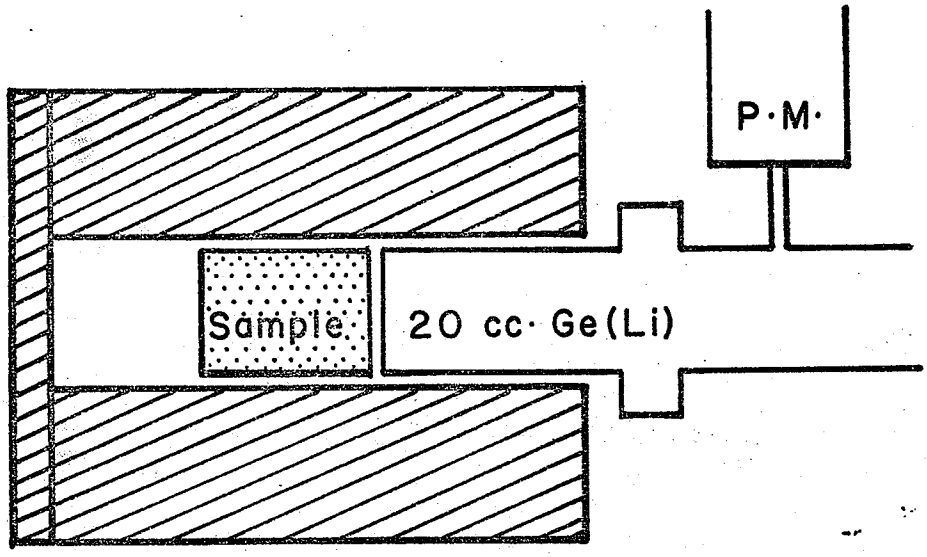
P·M·
Sample
20 cc· Ge(Li)

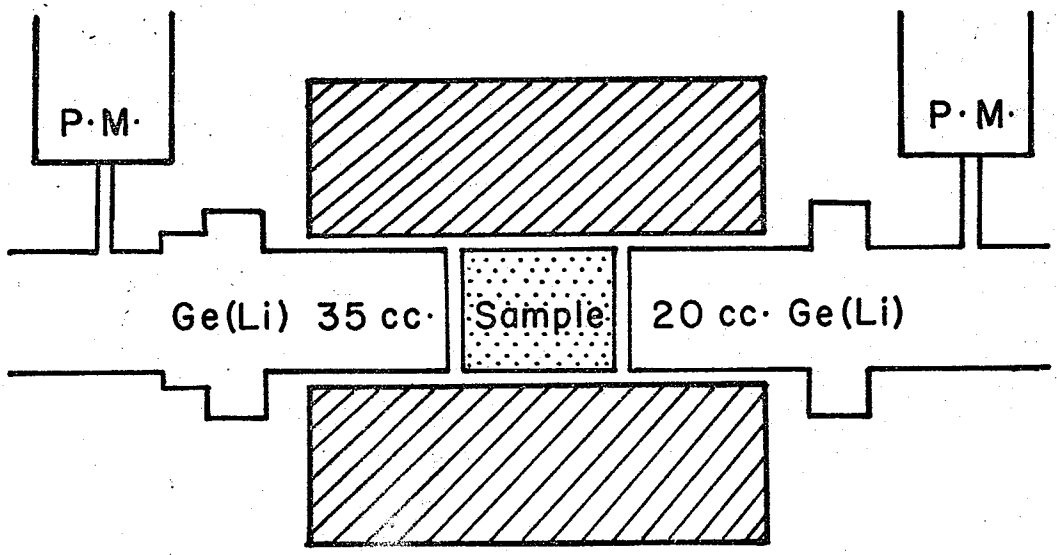
P·M·
P·M·
Ge(Li) 35 cc·
Sample
20 cc· Ge(Li)

Figure III-3

Typical Gamma Spectrum of the Rock Samples.

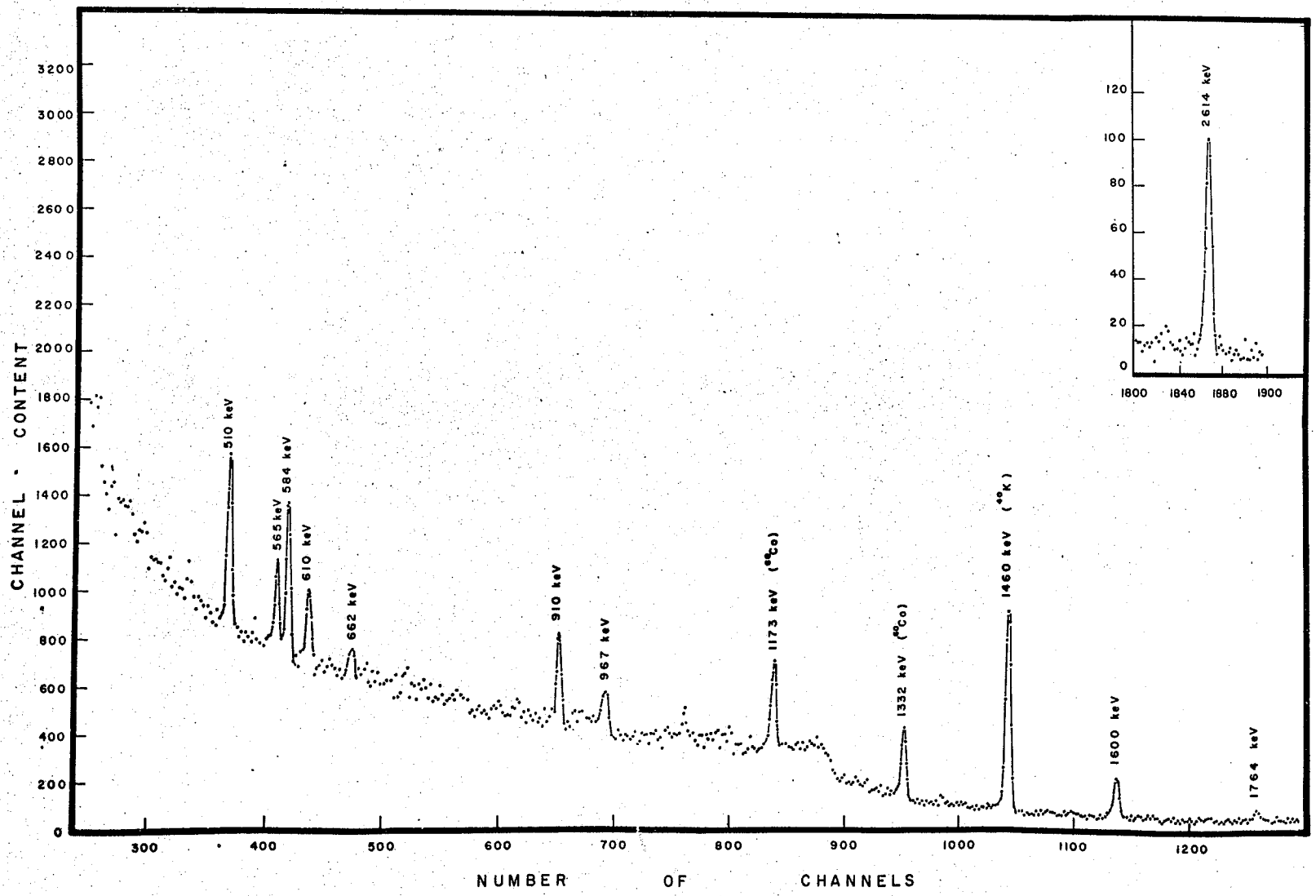
CHANNEL - CONTENT
NUMBER OF CHANNELS
510 keV
565 keV
584 keV
610 keV
662 keV
910 keV
967 keV
1173 keV (60Co)
1332 keV (60Co)
1460 keV (40K)
1600 keV
1764 keV
2614 keV

It was found that the bricks of the walls of our laboratory contain traces of potassium. As a result, a blank run without any sample inside the shield was made, to determine the contribution of potassium from the wall. The area of the 1460 keV peak obtained this way was subsequently subtracted from all the potassium peaks as background radiation.

The method of handling background had already been dealt with in Chapter I. The method of error analysis was due to the late Dr. Roulston, and is presented in Appendix IV.

III.5 RESULTS AND DISCUSSION

The resultant concentrations of the trace elements are presented in Table III-4. A plot of the relative abundance is shown in Figure III-4.

Note roughly the linear correspondance of FM-31, 1, 100, 68 at a high Th/U ratio ($\gtrsim$10). The trend is from Lac du Bonnet quartz manzonite to hybrid or marginal porphyritic to pegmatite in order of increasing Th and U abundance, and decreasing Th/U ratio. The high characteristic Th/U ratio is correlated with a notable abundance of accessory allanite (a Th carrier). The enrichment of U relative to Th, progressing to the pegmatite phase, is consistant with the idea[3],[4] that oxidizing fluids which finally deposited the pegmatite were preferentially enriched in U relative to Th.

If a limit of 1 ppm of U is put on FM-24, there is

Table III-4

U,Th, and K contents of the Rock Samples.

SAMPLE	LOCALITY Latitute (N.); Longitute (W.)	Rock Type	U p.pm	Th p.pm	K %	Th/U
FM- 1	49° 38' ; 95° 40'	Adamellite	3·7±13 %	38·1±6 %	5·5±3.2%	10·3
FM-31	50° 17' ; 95° 52'	Adamellite	2·5±5·3 %	32·2±6 %	5·6±2·8 %	13·
FM-27	49° 43' ; 94° 52'	Aplite	11·4±5·5%	15·9±7·7%	4·9±2·7 %	1·4
FM-100	50° 07' ; 95° 39'	Adamellite	5·1±8·9 %	57·9±5 %	5· ±5 %	11·4
FM-68	49° 37' ; 95° 36'	Pegmatite	11·2±5·6 %	96·7±4 %	3·3±3·2 %	9·
FM-14	49° 38' ; 95° 04'	Aplite	3·2±13 %	21·7±5·7%	4·8±2·4 %	6·7
FM-24	49° 43' ; 94° 52'	Granodiovite		7· ±9 %	2·5±2·7 %	
FM-22	49° 44' ; 94° 54'	Gneiss	28·1±4·6%	22·2±10 %	5·7±3·3 %	0·7

Figure III-4

Plots of Th vs. U

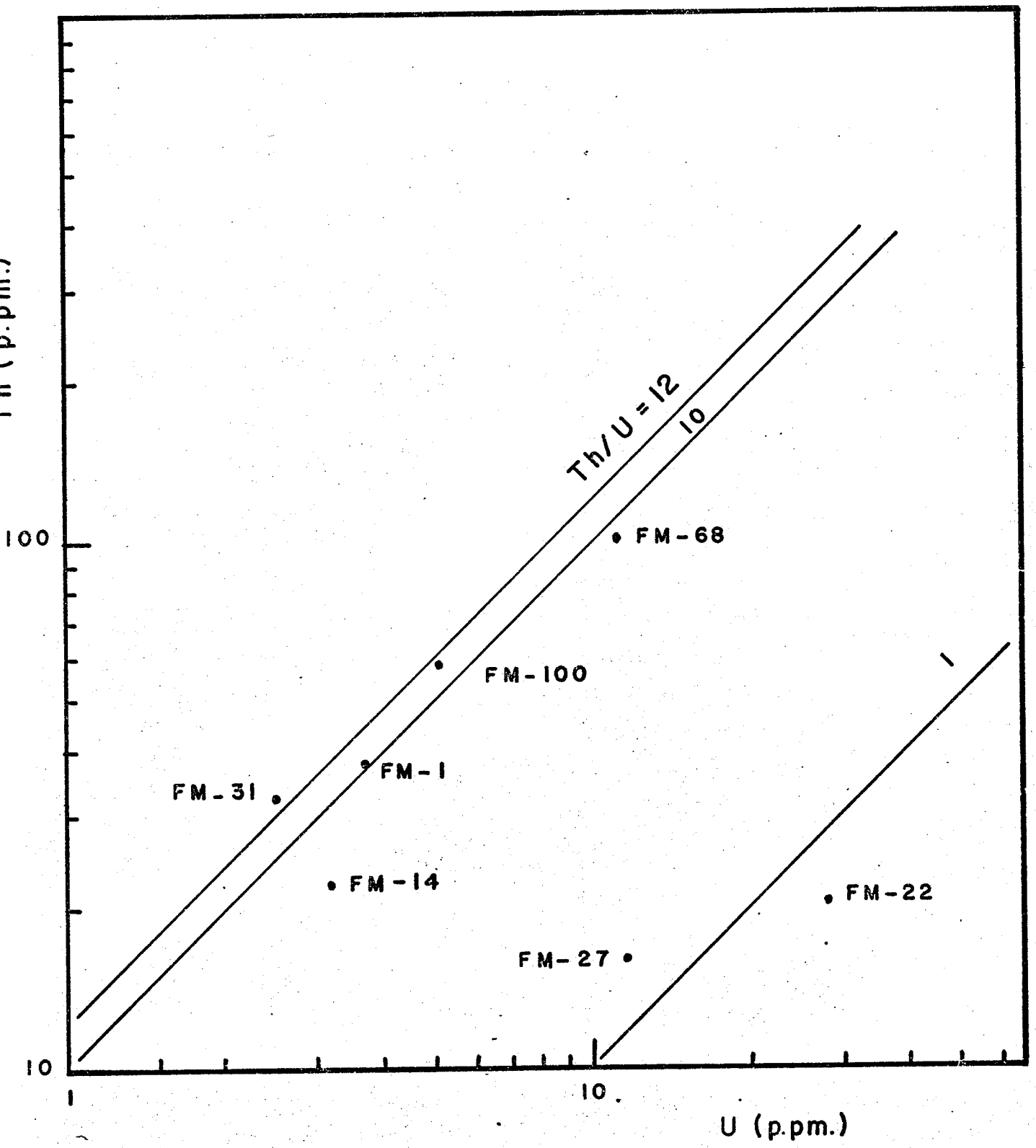
Th (p.ppm.)
100
10
1
10
U (p.ppm.)
Th/U = 12
10
1
FM-68
FM-100
FM-1
FM-31
FM-14
FM-22
FM-27

a similar enrichment in U relative to Th in the later cross-cutting aplite in FM-27. The nearby gnesis (FM-22) has a markly low Th/U ratio which may reflect the nature of the original material. Alternatively, the enrichment of U may reflect the gain of U^{6+} during the process of re-mobilization referred to earlier. Thus, FM-14, a cross cutting aplite, is predictably enriched in U and Th, but it is impossible to say if it is due to preferentially enrichment in U.

The accuracy of gamma-ray spectroscopy method, using Ge(Li) detectors, is good, and is certainly adequate for this type of analysis. Higher resolution makes it possible to determine the concentrations with accuracies many times better than similar work done with NaI crystals. The only drawback is that the detection efficiencies of Ge(Li) detectors is usually a few per cent of that of a 3X3 NaI, hence the time of collection of data is longer than that of NaI by as much as a factor of 20, thereby making field measurements extremely impractical, not to mention the care require to ensure the safety of the cryostat, supply of liquid nitrogen etc. However, if the rock samples can be brought to the laboratory, solid state detectors are indispensible for accurate work. Further, computer programs may be used for the systematic analysis of data, which will save a lot of time at the desk calculator. In conclusion, it should be pointed out that more samples are necessary for full scale geological survey. The present work shows merely, for the first time, how the solid state detectors can be used to investigate, very accurately, the concentration of trace elements in the naturally radioactive rocks.

III.6 REFERENCES, CHAPTER III

1) E.S.Moore, "Region East of the South End of Lake Winnipeg". Geol. Surv. Can. Summ. Report.(1912) pge 262-270.

2) J.C.Davis (1965), "Geology of High Lake-Rush Bay Area". Ont. Dept. of Minerals. Geology Report#41, pge 51.

3) R.B.Farguharson, Private communication (1969).

4) K.S.Heier, W.Compston and I.McDougall, Geochimica et Cosmochimica Acta, 29, 643 (1965).

5) R.Narayanaswamy and V.S.Venkatasubramanian, Geochimica et Cosmochimica Acta, 33, 1007 (1969).

APPENDIX I

To a first approximation, the statistical distribution in the number of ion-pairs created by a gamma ray of energy E, is nearly Gaussian. Analytically, it can be described by the function f(x), where

$$f(x) = Ae^{-\frac{(x-\bar{x})^2}{2\sigma^2}}$$

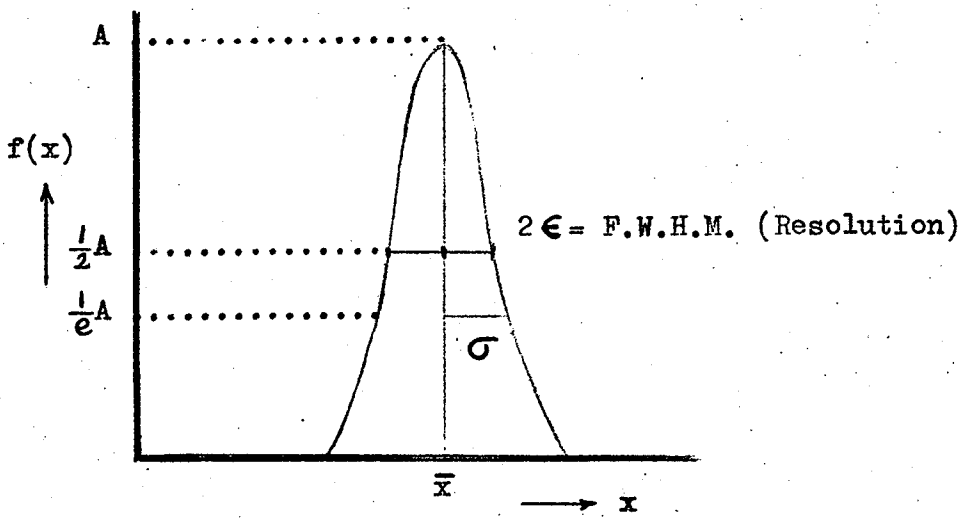

Here σ^2 is the variance. In practice, it is convenient to talk about the full width half maximum (F.W.H.M.), as indicated by 2ϵ in the above diagram, defined by

$$\tfrac{1}{2}A = A\, e^{\epsilon^2/2\sigma^2}$$

that is

$$\log_e 2 = \frac{\epsilon^2}{2\sigma^2}$$

or

$$\epsilon^2 = 2(\log_e 2)\sigma^2$$

Hence

$$2\epsilon = 2\sqrt{2 \log_e 2}\,\sigma = 2.35\sigma$$

APPENDIX II

FLOW CHART OF DATA ANALYSIS PROGRAMME.

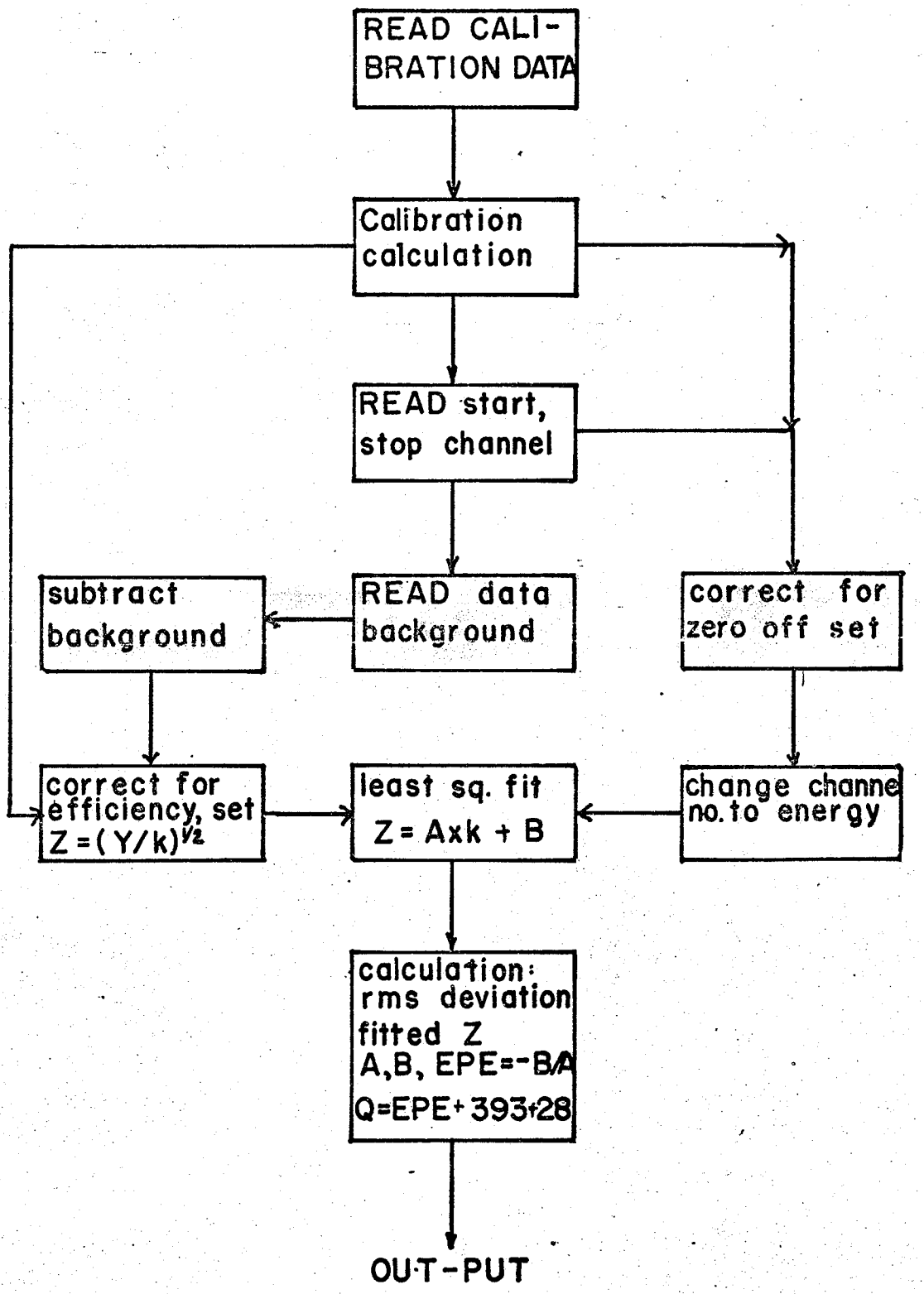
READ CALI-
BRATION DATA
Calibration
calculation
READ start,
stop channel
READ data
background
subtract
background
correct for
zero off set
correct for
efficiency, set
Z = (Y/k)^1/2
least sq. fit
Z = Axk + B
change channe
no. to energy
calculation:
rms deviation
fitted Z
A,B, EPE=-B/A
Q=EPE+393+28
OUT-PUT

APPENDIX III

THEORY OF LEAST SQUARES

The problem of least squares arises when one looks for a convenient way of treating one's experimental data, as well as providing a useful means of determining experimental error. A function of physical or theoretical significance is usually known, and the best value for the parameters of this function is desired.

We begin by assuming that we have a function of the form:

$$y = f(x_1,.....x_m ; \alpha_1,.....\alpha_p) \qquad (1)$$

where

$(x_1,.....x_m)$ is a set of n observations,

and $(\alpha_1,.....\alpha_p)$ is a set of p parameters to be determined.

y is the dependent variable, while

x_i are the independent variables.

Our problem is to determine the parameters $(\alpha_k,\ k=1,\cdots p)$. There are many possible ways of doing it, and we choose a method such that the sum of the squares of the deviations of the observables y_i from the function $f(x_i, \alpha_j)$ is a minimum. Mathematically, this means that we wish to minimize Q where

$$Q = \sum_{i=1}^{n} w_i \left[y_i - f(x_{1_i},\ldots x_{m_i} ; \alpha_1,\ldots \alpha_p) \right]^2 \qquad (2)$$

Here, n is the number of observables, and $n > p$,

w_i are the weighting factors.

From a purely formal standpoint, we can minimize Equ.(2), by differentiating Q with respect to α_k , k=1,...p and equating to zero, and solving the resulting set of p simultaneous equations. e.g.:

$$\frac{\partial Q}{\partial \alpha_k} = -2 \sum_{i=1}^{n} w_i \left[\left(\frac{\partial f}{\partial \alpha_k}\right)_i \; y_i - f(x_{1_i} \ldots x_{m_i}; \alpha_1 \ldots \alpha_p) \right] = 0 \tag{3}$$

where $\left(\frac{\partial f}{\partial \alpha_k}\right)_i$ denotes the value of the i^{th} partial derivatives for the i^{th} data point.

Rearranging Equ.(3), and setting $f_i = f(x_i, \alpha_1 \ldots . \alpha_p)$ we obtain the more useful form:

$$\left.\begin{aligned}
\sum_{i=1}^{n} w_i \; f_i \left(\frac{\partial f}{\partial \alpha_1}\right)_i &= \sum_{i=1}^{n} w_i y_i \left(\frac{\partial f}{\partial \alpha_1}\right)_i \\
\sum_{i=1}^{n} w_i \; f_i \left(\frac{\partial f}{\partial \alpha_2}\right)_i &= \sum_{i=1}^{n} w_i y_i \left(\frac{\partial f}{\partial \alpha_2}\right)_i \\
&\vdots \\
\sum_{i=1}^{n} w_i \; f_i \left(\frac{\partial f}{\partial \alpha_p}\right)_i &= \sum_{i=1}^{n} w_i y_i \left(\frac{\partial f}{\partial \alpha_p}\right)_i
\end{aligned}\right\} \tag{4}$$

Equations(4) are known as the normal equations. Note that they

are, in general, a system of p non-linear equations, and there is no garantee that a solution exists, or that if a solution does exist, that is to be unique. However, in the case where α_k, $k=1,\ldots p$ appears as linear coefficients of the independent variables, a unique solution is always guaranteed, with somewhat less stringent restrictions.

In our particular case, we are interested in performing the fit to the function:

$$y_i = ax_i + b \tag{5}$$

where y_i is the dependent variable (in fact, $y_i = \sqrt{\frac{N(k)}{k}}$)
x_i is the i^{th} independent variable to be identified with the i^{th} channel (at energy k).
Assuming equal weight for the time being for the sake of convenience of discussion, the quantity Q we want to minimize is

$$Q = \sum_i^n \left[y_i - (ax_i + b) \right]^2 \tag{6}$$

and the normal equations can be written in the form:

$$\begin{aligned} a \sum_i x_i^2 + b \sum_i x_i &= \sum_i x_i y_i \\ a \sum_i x_i + bn &= \sum y_i \end{aligned} \tag{7}$$

which can be summarized by the matrix equation:

$$X\,Y = Z \tag{8}$$

where

$$X = \begin{pmatrix} \sum_i x_i^2 & \sum_i x_i \\ \sum_i x_i & n \end{pmatrix}; \quad Y = \begin{pmatrix} a \\ b \end{pmatrix} \quad ; \quad Z = \begin{pmatrix} \sum_i x_i y_i \\ \sum_i y_i \end{pmatrix}$$

Note that X is symmetric, and provided it is non-singular (that is, its determinant is not equal to zero), the solution can be obtained simply:

$$Y = X^{-1}Z \tag{9}$$

The above method had been used for the Kurie type fit. In fact, this method can handle a large number of problems, sometimes with suitable transformations. The versitility of the University computer enables a large number of parameters to be determined. A number of 'package' programs are also available for solving linear types of least square problems.

APPENDIX IV

ERROR ANALYSIS

In this appendix, we shall present a method of error analysis on the data of the geochemical experiments. Suppose N_1 is the total number of counts under the peak, (including background),

and $N_2 = n \times N_b$

where n is the number of channels under the peak and N_b is average background.

Area of the peak = $N_1 - N_2$

Then the standard deviation:

$$\sigma_1(\text{in } N_1) = N_1$$

N_b is the average of a number of channels (n_b).

Then, $\sigma_b = \sqrt{N_b n_b}$ is the standard deviation in background, and fractional

$$\sigma_b = \frac{1}{\sqrt{N_b n_b}}$$

So that,

$$\sigma_2 = n\, N_b \frac{1}{\sqrt{N_b n_b}}$$

In the standard deviation associated with the area determination of the peak is

$$\sigma_{(N_1-N_2)} = \sqrt{\sigma_1^2 + \sigma_2^2}$$

$$= \sqrt{N_1 + \frac{n^2 N_b^2}{N_b n_b}}$$

$$= \sqrt{N_1 + \frac{n^2}{n_b} N_b}$$

We define, the % error = $\frac{\sigma_{(N_1 - N_2)}}{N_1 - N_2} \times 100\ \%$

This is believed to be a reasonable estimation of experimental error. A usual figure is $\simeq 6\ \%$.